Reactor Modelling for Fluid-Solid Systems

Vincenzo Russo

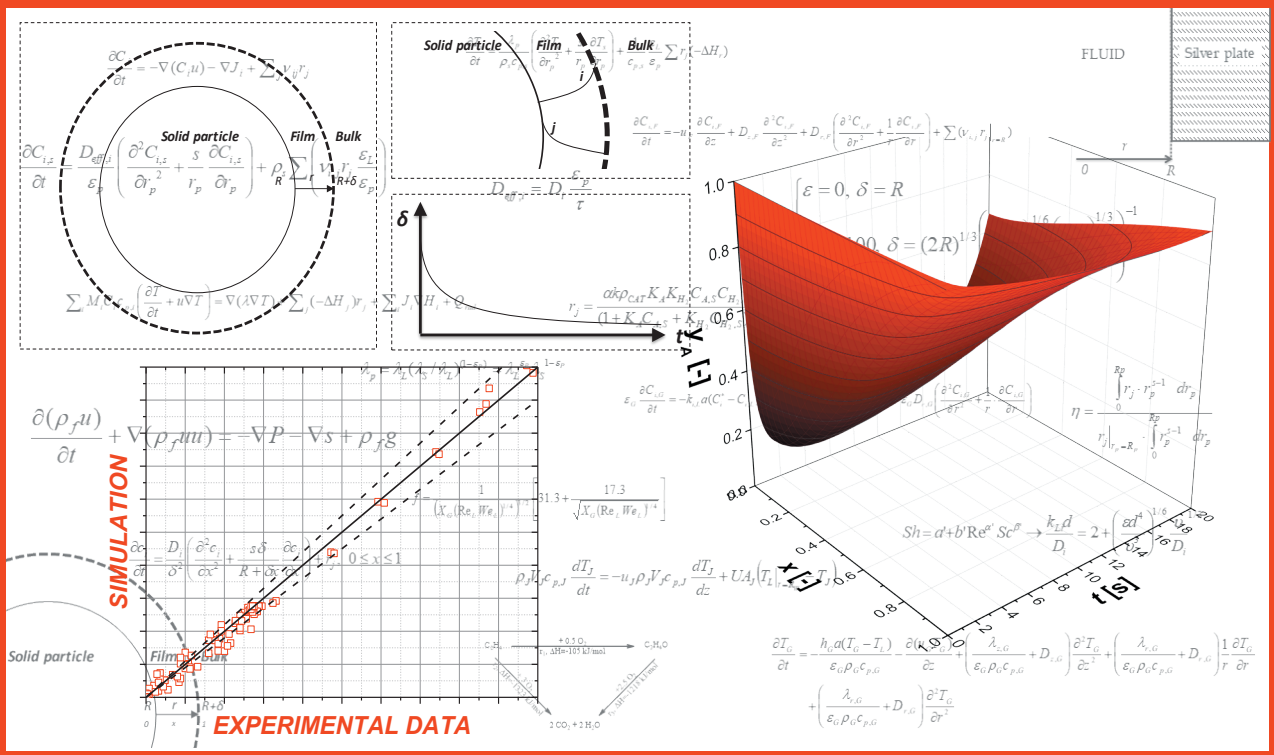

Laboratory of Industrial Chemistry and Reaction Engineering
Johan Gadolin Process Chemistry Centre
Faculty of Science and Engineering
Åbo Akademi University

Åbo Akademi

Vincenzo Russo, PhD

- 43 papers, 2 book chapters
- *h*-index = 10
- 333 total citations by 248 documents
- Scopus database: 37018701000
- ORCID: http://orcid.org/0000-0002-1867-739X

Academic titles

PhD in Chemical Sciences, May 9th 2014. University of Naples Federico II.

Thesis title: *"Kinetic and Catalytic Aspects in Propene Oxide Production"*

Master of Science in Industrial Chemistry, June 23rd 2010. University of Naples Federico II.

Thesis title: *"New methods for Epoxidized Soybean Oil production"*

Bachelor of Science in Industrial Chemistry, March 28th 2008. University of Naples Federico II.

Thesis title: "*Epoxidation processes in micro reactors: preliminary evaluations"*

Research field of interest

Reaction and reactor modelling of multiphase systems

Kinetic investigation of catalytic reactions

Safety criteria for exothermic reactions

Design and realization of lab-scale pilot plants

Plant automation and control

Reactor Modelling for Fluid-Solid Systems

Vincenzo Russo

Laboratory of Industrial Chemistry and Reaction Engineering
Johan Gadolin Process Chemistry Centre
Faculty of Science and Engineering / Chemical Engineering
Åbo Akademi University
2017

Supervised by

Professor Tapio O. Salmi
Laboratory of Industrial Chemistry and Reaction Engineering
Åbo Akademi University

Professor Dmitry Yu. Murzin
Laboratory of Industrial Chemistry and Reaction Engineering
Åbo Akademi University

ISBN 978-952-12-3597-9 (printed)
ISBN 978-952-12-3598-6 (PDF)
Painosalama Oy – Turku, Finland 2017

To my grandfather, who didn't live enough to enjoy my goals.

Preface

The present PhD thesis is the result of a long and fruitful period spent at the Laboratory of Industrial Chemistry and Reaction Engineering of Åbo Akademi, dealing with reactor modelling for fluid-solid systems. A wide variety of scientific problems have been faced and the main results published. Writing a PhD thesis means certainly to achieve a big goal, result of hard work and learning. This would not be possible in the absence of the right environment, culture and dedication.

When you meet scientists of the right caliber then things get easier, and I have been lucky and honored to work in cooperation with Professor Tapio O. Salmi. My warmest gratitude goes to him, who taught me the right approach to the rigorous interpretation of physical and chemical phenomena in modelling and designing chemical reactors. Professor Dmitry Yu. Murzin with his experience and dedication to the work taught me the meaning of perseverance. Doctor Kari Eränen and Professor Johan Wärnå have been of inspiration if facing both technical and numerical problems.

The top researchers, Doctors Henrik Grénman, Pasi Tolvanen, Teuvo Kilpiö and Atte Aho have been good friends and excellent colleagues. I am sure that we will do great things together.

My warmest thanks go to my family, who supported me in the period when I was in Turku. To my very best friends, Mirko, Rosa, Rosita who dedicated to me as much time as possible in my short visit in Napoli. To my professors in Napoli, Martino Di Serio and Riccardo Tesser, who trusted in me and supported me in this experience. And to you, Flavia… the kilometers separating each other were really a lot, but I am sure that it never happened in the history that such a long and tough line, namely our love, was able to connect Turku and Napoli.

Turku/Åbo, June 2017

Vincenzo Russo

Abstract

Reactor Modelling for Fluid-Solid Systems

The aim of the present doctoral thesis is the development of reliable mathematical models for the simulation of fluid-solid reactors. The main idea was to elaborate a rigorous general non-isothermal three-phase tubular reactor model. The evolution of both concentration and temperature profiles was along all the four coordinates constituting the reactor itself, i.e.: (i) reactor length, (ii) reactor radius, (iii) radius of each particle located inside each position of the reactor, (iv) time. The model was developed to be switchable, giving the possibility to derive sub-models by setting some parameters at zero.

Different sub-models were tested on real case studies, and good results in terms of data interpretation were obtained. Each chapter of this thesis is dedicated to the presentation of a model/sub-model with a related application to a practical case study. The general model was applied to an exothermic three-phase reaction performed in a laboratory-scale trickle bed reactor. The simultaneous solution of both mass and heat balances was described in detail. The tested sub-models were either two-phase or single-phase models. In particular, two microreactor models were developed for the partial oxidation of ethylene, and a two-phase packed bed reactor for the partial oxidation of ethanol.

The final chapter describes the results of a special liquid-solid system, where the solid acts as a reactant and diminishes in size as the reaction progresses. The reaction was considered to proceed simultaneously both in the stagnant film surrounding the solid particle and in the bulk phase of the liquid. As the reaction proceeds, the particle radius shrinks and the stagnant film becomes thinner. An approach was presented for a development of a shrinking particle model, where the problem of the moving boundary was successfully solved. The model was applied to a real case, that is the limestone dissolution, obtaining good results.

The developed models will be the basis for future application on both laboratory and industrial scale reactors.

Referat

Reaktormodellering för fluid-fastfassystem

Denna doktorsavhandling har som mål att utveckla tillförlitliga matematiska modeller för simulering av vätske-fastfasreaktorer. Den dominerande idén har varit att utarbeta rigorösa och allmänna icke-isotermiska modeller för rörreaktorer, där tre faser förekommer. Koncentrations- och temperaturgradienter förekommer i fyra dimensioner i reaktorer, d.v.s. reaktorlängd (i), reaktorradie (ii), partikelradie i varje partikel i reaktorn (iii) och tid (iv). Modellen utvecklades så att det finns en flexibel möjlighet att övergå till betydligt enklare undermodeller genom att sätta valda parametervärden till noll.

Olika undermodeller testades för reella fall och goda resultat nåddes då experimentella data tolkades med hjälp av modellerna. Varje kapitel i denna avhandling är tillägnat en modell eller en undermodell som är relaterad till ett praktiskt experimentellt fall. Den allmänna modellen tillämpades på en exotermisk trefasreaktion som var genomförd i en tricklebäddreaktor i laboratorieskala. Den simultana lösningsmetodiken av både mass- och energibalanser beskrevs i detalj. De testade undermodellerna var antingen tvåfas- eller enfasmodeller. Två mikroreaktor-modeller utvecklades för partiell oxidation av eten och en tvåfasreaktormodell för en packad bädd som användes för oxidation av etanol.

Det sista kapitlet beskriver resultaten från ett speciellt vätske-fastfassystem, där den fasta fasen fungerar som reaktant och minskar i storlek då reaktionen framskrider. Reaktionen antogs pågå samtidigt både i den stillastående filmen runt den fasta partikeln och i vätskans huvudmassa. Då reaktionen framskrider, minskar partikelradien och den stagnanta filmen runt partikeln blir tunnare. En krympande partikelmodell utvecklades, i vilken problemet med en rörlig fasgräns framgångsrikt löstes. Modellen tillämpades på ett reellt fall, upplösning av kalksten och goda resultat erhölls.

De modeller som utvecklades, kommer att utgöra grunden för framtida tillämpningar för reaktorer i laboratorieskala och industriell skala.

Sinossi

Modellazione di reattori per sistemi Fluido-Solido

Lo scopo della presente tesi di dottorato è lo sviluppo di modelli matematici realistici per la simulazione di reattori fluido-solido. L'idea principale è quella di sviluppare un modello rigoroso di un reattore trifasico non isotermo. È stata ottenuta l'evoluzione dei profili di concentrazione e temperatura lungo le quattro coordinate costituenti il reattore stesso: (i) lunghezza del reattore, (ii) raggio del reattore, (iii) raggio di ciascuna particella collocata in ogni posizione del reattore stesso, (iv) tempo. Il modello è stato sviluppato al fine di essere adattabile, dando la possibilità di derivare sotto-modelli settando a zero alcuni parametri.

I diversi sotto-modelli sono stati testati su casi studio reali, ottenendo buoni risultati in termini di interpretazione di dati sperimentali. Ogni capitolo della tesi è dedicato alla presentazione di un modello/sotto-modello e la relativa applicazione a un caso reale. Il modello generale è stato applicato a una reazione esotermica trifasica, condotta in un reattore "trickle bed" da laboratorio. La soluzione simultanea dei bilanci di materia ed energia è stata descritta in dettaglio. I sotto-modelli testati sono o bifasici o mono fasici. In particolare, due modelli di microreattori sono stati sviluppati per l'ossidazione parziale dell'etilene, mentre un reattore a letto fisso monofasico per l'ossidazione parziale dell'etanolo.

Nell'ultimo capitolo sono descritti i risultati di un sistema liquido-solido molto particolare, dove il solido agisce da reagente e diminuisce di dimensione col decorso della reazione. È stato supposto che la reazione possa procedere simultaneamente nel film di liquido stagnante che circonda la particella solida e nel bulk del liquido. Col procedere della reazione, il raggio della particella diminuisce e il film diventa più sottile. Viene presentato un approccio allo sviluppo di un modello particellare, dove il problema della condizione al contorno mobile viene risolto con successo. Il modello è applicato alla dissoluzione della calce, ottenendo risultati soddisfacenti. I modelli sviluppati saranno la base per future applicazioni per reattori sia in scala laboratorio che industriale.

List of Publications and Prize

The thesis consists of the following publications, which are referred to, in the text, by their Roman numerals.

I. T. Kilpiö, V. Russo, K. Eränen, T. Salmi. Design and modeling of laboratory scale three phase fixed bed reactors. *Physical Sciences Reviews* **2016**, 1(3), -. Online open access journal. doi:10.1515/psr-2015-0020.

II. V. Russo, T. Kilpiö, M. Di Serio, R. Tesser, E. Santacesaria, D. Y. Murzin, T. Salmi. Dynamic non-isothermal trickle bed reactor with both internal diffusion and heat conduction: arabinose hydrogenation as a case study. *Chemical Engineering Research and Design* **2015**, 102, 171-185.

III. V. Russo, T. Kilpiö, J. Hernandez Carucci, M. Di Serio, T. Salmi. Modeling of microreactors for ethylene epoxidation and total oxidation. *Chemical Engineering Science* **2015**, 134, 563–571.

IV. T. Kilpiö, E. Behravesh, V. Russo, K. Eränen, T. Salmi. Physical Modelling of the Laboratory-Scale Packed Bed Reactor for Partial Gas-Phase Oxidation of Alcohol using Gold Nanoparticles as the Heterogeneous Catalyst. *Chemical Engineering Research and Design* **2017**, 117, 448-459.

V. T. Salmi, V. Russo, C. Carletti, T. Kilpiö, R. Tesser, D. Murzin, T. Westerlund, H. Grénman. Application of film theory on the reactions of solid particles with liquids: shrinking particles with changing liquid films. *Chemical Engineering Science* **2017**, 160, 161-170.

VI. V. Russo, T. Salmi, C. Carletti, D. Murzin, T. Westerlund, R. Tesser, H. Grénman. Application of an Extended Shrinking Film Model to limestone dissolution. *Industrial & Engineering Chemistry Research* **2017**.

(I) V.R. contributed actively to the mathematical modelling and wrote parts of the article. (II) V.R. performed the mathematical modelling and wrote the manuscript. (III) V.R. made the modelling and wrote the manuscript. (IV) V.R. contributed to the implementation of the model in computations (V) V.R. made all the computations and wrote large parts of the article (VI) V.R. made the modelling and wrote the manuscript

Prize

PSE Model-Based Innovation Prize runner-up, 2015. Winning paper: V. Russo, T. Kilpiö, J. Hernandez Carucci, M. Di Serio, T. Salmi. Modeling of microreactors for ethylene epoxidation and total oxidation. *Chemical Engineering Science* **2015**, 134, 563–571.

Contents

Chapter 1 – Introduction

"In science, all facts, no matter how trivial or banal, enjoy democratic equality."

Mary McCarthy, The fact in Fiction, in On the Contrary, 1961

1.1 Modelling of chemical reactors

Modelling of chemical reactors is a specific sector of chemical engineering science, particularly chemical reaction engineering, dedicated to the description of all the chemical and physical aspects occurring inside a reactor. As the number of reactor types is very large, it is difficult to rationalize all the advances made in modelling[1]. The situation becomes even more complicated if we think that often for a same chemical process, different kinds of reactors can be used. For example, different processes have been proposed for methanol synthesis, where the core of the plant can be either a slurry reactor working under a fluidized state or packed bed reactor[2]. Multitubular reactors, fluidized bed and riser reactors are preferable used for heterogeneous catalytic oxidations[3].

Focusing on the phenomena appearing in a chemical reactor, it is possible to classify reactors, setting the basis on the development of dedicated mathematical models. A first general classification can be made as follows:

- Batch and semi batch reactors
- Continuous stirred tank reactors
- Continuous tubular reactors
    - Plug-flow, laminar flow, non-ideal flow
    - Packed bed, trickle bed
- Fluidized bed reactors

The classification is certainly oversimplified, when considering that many books[1,4,5,6], monographies and review articles have been published on the topic, few pages of a PhD thesis introduction can just give an idea on the general variety.

---

[1] G.F. Froment, K.B. Bischoff, J. De Wilde. Chemical Reactor Analysis and Design (3rd edition). John Wiley & Sons Inc., New York: **2001**.

[2] J.A. Moulijn, M. Makkee, A. van Diepen. Chemical Process Technology. John Wiley & Sons, Ney York: **2001**.

[3] D.Yu. Murzin. Chemical Reaction Technology. Walter de Gruyter, Berlin: **2015.**

[4] T. Salmi, J.-P. Mikkola, J. Wärnå. Chemical Reaction Engineering and Reactor Technology. CRC Press, New York: **2010**.

[5] B. Saha. Catalytic Reactors. Walter de Gruyter, Berlin: **2016**.

[6] P.A. Ramachandran, R.V. Chaudari. Three-Phase Catalytic Reactors. Gordon and Breach Science Publishers, New York: **1983**.

Independent of the reactor equipment, the physical phenomena occurring in a chemical reactor can be always classified in:

- Reaction
- Mass transfer
- Heat transfer
- Momentum transfer

Quantitative describe a reactor implies writing down the basic equations needed to describe the mentioned phenomena, namely the conservation equations for mass, heat and momentum.

The derivation of a differential mass balance, also called mass continuity equation, for an arbitrary component i present in a fluid element is generally given by Eq. 1[7,8].

$$\frac{\partial C_i}{\partial t} = -\nabla(C_i u) - \nabla J_i + \sum_j \nu_{ij} r_j \qquad (1)$$

The presented terms refer respectively to

- Accumulation: $\partial C_i / \partial t$
- Convective flow: $\nabla(C_i u)$
- Chemical reaction rates: $\sum_j \nu_{ij} r_j$
- Flux given by molecular diffusion: ∇J_i

Ideally, with this general equation, it would be in principle possible to model every reactor case. For example, for a batch reactor, the accumulation and the reaction rate are the only terms to be considered, while for a dynamic plug-flow reactor it is necessary to introduce also the convective term. For multiphase systems, it is necessary to write a mass balance for each phase, including terms related to interfacial mass transfer. J_i represents the molar flux vector with respect to the mass-average velocity. Depending on the reactor type, it can assume different

[7] R.B. Bird. The Equations of Change and The Macroscopic Mass, Momentum, And Energy Balances. *Chem. Eng. Sci.* **1957**, *6*, 123-131.
[8] R.B. Bird, W.E. Stewart, E.N. Lightfoot. Transport Phenomena (2nd edition). John Wiley & Sons Inc., New York: **2007**.

forms (i.e. Fick's law for laminar reactors, axial and radial dispersion terms for turbulent reactors). In the case of multicomponent diffusion in gases at low density, the Maxwell-Stefan equations were formulated, stating that the diffusion flux is given by the deviation from equilibrium between the thermodynamic interactions and molecular friction, this last proportional to the difference in speed and their mole fractions of two components[8].

In an analogous way, the general energy balance equation can be written as Eq. 2[8].

$$\sum_i M_i C_i c_{p,i}\left(\frac{\partial T}{\partial t} + u\nabla T\right) = \nabla(\lambda \nabla T) + \sum_j (-\Delta H_j) r_j + \sum_i J_i \nabla H_i + Q_{rad} \quad (2)$$

The presented terms refer to

- Accumulation: $\partial T / \partial t$
- Convective flow: $u\nabla T$
- Heat transfer by conduction: $\nabla(\lambda \nabla T)$
- Chemical reaction effect: $\sum_j (-\Delta H_j) r_j$
- Energy flux by molecular diffusion: $\sum_i J_i \nabla H_i$
- Radiation heat flux: Q_{rad}

Finally, the general momentum transfer balance equation can be described by the Navier-Stokes equations, Eq. 3.

$$\frac{\partial(\rho_f u)}{\partial t} + \nabla(\rho_f uu) = -\nabla P - \nabla s + \rho_f g \quad (3)$$

The description of all the terms is

- Accumulation: $\partial(\rho_f u) / \partial t$
- Convection: $\nabla(\rho_f uu)$
- Pressure gradient: ∇P
- Shear stress: ∇s
- Gravity: $\rho_f g$

The reactor models published in the literature are often written by simplifying the mass and energy balance equations, adapting it to the

case of interest[9],[10]. Instead, the momentum balance equation is usually omitted. Instead, solving the velocity profiles are solved with algebraic expressions (i.e. parabolic profiles for laminar flow model) and the pressure drop is often calculated by using friction factor correlations[11]. This aspect is clearly seen when using code-based software. For computational fluid dynamics (CFD), the Navier-Stokes equation is normally included. The differences between the two approaches are the topic of the section 1.2.

Modeling a chemical reactor is not only a selection of terms to add to or remove from a continuity equation. One of the major difficulties is to understand how to write the terms. As an overview, some major issues concerning fixed bed reactor modeling are summarized in Table 1.

Further details and discussion on the topic can be found in **Publication I**. From the presented overview, the modelling of fluid-solid fixed bed reactors still remains a challenge for each new reaction system, because the individual effects are very case specific and strongly dependent on the actual operating conditions.

[9] S.F.A. Halim, A.H. Kamaruddin, W.J.N. Fernando. Continuous Biosynthesis of Biodiesel From Waste Cooking Palm Oil In A Packed Bed Reactor: Optimization Using Response Surface Methodology (RSM) And Mass Transfer Studies. *Bioresource Technology* **2009**, *100*, 710-716.

[10] Y. Seo, W.H. Hong. Kinetics of Esterification of Lactic Acid with Methanol In The Presence Of Cation Exchange Resin Using A Pseudo-Homogeneous Model. *Journal of Chemical Engineering of Japan* **2000**, *33(1)*, 128-133.

[11] M. Al-Dahhan, F. Larachi, M. Dudukovic, A. Laurent. High-Pressure Trickle Bed Reactors: A Review. *Ind. Eng. Chem. Res.* **1997**, 36, 3292-3314.

Table 1 – Main aspects to be considered in fluid-solid modelling.

Solid phase	1. Rate laws and temperature dependencies 2. Adsorption/desorption phenomena 3. Catalyst deactivation 4. Intraparticle diffusion limitation 5. Fluid-solid mass transfer limitation 6. Change in the physical nature of the fluid-solid film 7. Formation of a solid shell of another solid compound 8. Non-uniform active phase 9. Effective diffusivity determination 10. Effective thermal conductivity determination 11. Particle size distribution *12.* Irregular particle shapes
Fluid phase	1. Direction of the fluid 2. Non-idealities of the flow 3. By-passes and stagnant zones 4. Pressure drop 5. Hold-up 6. Physical properties determination 7. Axial and radial dispersion parameters 8. Interfacial mass transfer from a fluid phase to an another one

The complication increases when multiple reactions proceed simultaneously in each phase, and particles appear in various sizes and irregular shapes.

1.2 Modelling strategies for fluid-solid systems

Interpretation of fluid-solid systems is a hot topic in the chemical engineering field. Two main possibilities are nowadays available to describe the physical and chemical aspects involved in a fluid-solid reactor: computational fluid dynamics calculations (CFD)[12,13,14] or studies where the fluid dynamics of the reactor is described by simpler terms[11]. Both approaches have their merits and limitations.

CFD is surely an extremely powerful tool. Different high-level software is available (COMSOL Multiphysics, OpenFoams, Ansys Fluent), most of them are user friendly, and provide reliable simulation results. This software is mainly used for modelling non-idealities in the flow, for systems with a simplified regular geometry[15]. CFD modelling studies are most typically used for calculating flow profiles, pressure drop and liquid hold-up. Despite these advantages, single-phase CFD models for simple geometries are well-converging within an hour, without reactions. It can be difficult to predict how much more time is needed when non-linear reaction rate expressions are incorporated. The main drawback is that CFD demands heavy computations, especially when making free surface modelling dealing with three-phase systems. This fact is of particular relevance when running with parameter estimation problems, where a large number of simulations is needed to iteratively reach the minimum of the objective function. We believe that in the near future, this problem will be surmounted by the development of more rapid computers.

The alternative modelling approach facilitates the inclusion of more chemical and physical phenomena in reactor models, by describing the fluid dynamics in simpler terms. In this case, software devoted to the

[12] A. Atta, S. Roy, K. Nigam. A Two-Phase Eulerian Approach Using Relative Permeability Concept For Modelling Of Hydrodynamics In Trickle-Bed Reactors At Elevated Pressure. *Chem. Eng. Res. and Des.* **2010**, *88*, 369-378.

[13] Z. Kuzeljevic, M. Dudukovic. Computational Modelling of Trickle Bed Reactors. *Ind. Eng. Chem. Res.* **2012**, *51*, 1663-1671.

[14] Y. Wang, J. Chen, F. Larachi. Modelling and Simulation of Trickle-bed Reactors using Computational Fluid Dynamics: A State-of-the-Art Review. *Can. J. Chem. Eng.* **2013**, *91(1)*, 136-180.

[15] S. Schwidder, K. Schnitzlein. A New Model for the Design and Analysis of Trickle Bed Reactors. *Chem. Eng. J.* **2012**, *207-208*, 758-765.

self-code development is available (MATLAB, gPROMS ModelBuilder, Athena Visual Studio, C++, etc.). In this case the number of physical phenomena to be described depends on the user's decision, thus the computation time practically depends on it. This software normally provides faster computations compared to CFD, which is surely an advantage to be appreciated, especially in parameter estimation tasks. The risk of this approach is to end-up with oversimplified models that are not able to fully describe the physics of the system. These issues are of particular importance when scaling-up chemical reactors. It is not easy to avoid the generation of concentration and temperature gradients when working with industrial-scale reactors, i.e. to avoid a high pressure drop, large catalyst particles are normally used, therefore intraparticle diffusion limitation must be certainly considered. For the same reason, temperature gradients can arise inside the particle, while for laboratory-scale reactors it is easier to get isothermal conditions. Another important phenomenon neglected when simulating laboratory-scale reactors is radial diffusion and dispersion. Industrial reactors are often characterized by large diameters and low flow velocity, thus radial gradients should be considered. Flow-regimes, backmixing, pressure drop are other important features to take into account when scaling-up a reactor. Thus, a detailed model should include most of the mentioned terms. More details on the scale-up issues, along with some examples are reported in **Publication I**.

By considering that in code-typing the risk of typing errors always exist, much more attention must be paid compared to modern CFD software, where only initial and boundary conditions are needed, while the equations are most of the time treated as black boxes. This fact does not imply that CFD computations are easy to implement, on the contrary the choice of the right physics packages, the solvers, the mesh of calculation points (finite elements method), the geometry are challenging tasks to be faced. Another important aspect is that when modelling with rapidly running program codes, a multitude of test computations can be performed and an abundant amount of feedback is received. With CFD, the number of trials becomes limited. For these reasons, in the present work, the attention was focused on the code-based approach.

A lot of effort has been made on the field, as reported in scientific literature[16,17,18,19]. Even if the first studies are rather old and reactor models, dealing with the most common fluid-solid problems, have been developed, most of them are far from reliable and the mathematical solution of the involved mass and heat balances is only approximate. As a matter of fact, most of the studies dealing with mathematical models for fluid-solid chemical reactors focus on the details of one or few individual effects, i.e. axial dispersion models, packed bed with fluid-solid external mass transfer limitation, or non-isothermal packed bed reactors. Even a simpler approach has been used, by adopting rigorous analytical solutions, which are valid in only a fixed range of operation conditions. The risk is that, the predictive power of such kind of models can be very low.

The aim of the present thesis is to develop reliable reactor models for fluid-solid systems, by using one of the classical code-based software, namely gPROMS ModelBuilder. The strategy is overviewed in next section.

1.3 Aim and approach

Two main reactor models were developed in this doctoral thesis:

- Heat exchanged gas-liquid-solid continuous reactor
- Fluid-solid batch reactor for dissolution kinetics

The original idea behind the generation of a comprehensive tubular reactor model was not only to use the final model as it was developed, but also to make it flexible, in a very general way, which means to generate all the simpler derivable sub-models by setting various terms off (Figure 1).

---

[16] A.G. Dixon. Fixed Bed Catalytic Reactor Modelling-The Radial Heat Transfer Problem. *The Canadian Journal of Chemical Engineering* **2011**, *90(3)*, 507-527.

[17] W.R. Paterson, J.J. Carberry. Fixed Bed Catalytic Reactor Modelling: The Heat Transfer Problem. *Chemical Engineering Science* **1983**, *38(1)*, 175-180.

[18] R.J. Dry. Fluidised Beds of Fine, Dense Powders: Scale-Up and Reactor Modelling. *Powder Technology* **1985**, *43(1)*, 41-53.

[19] J. Villadsen. Challenges and Cul-De-Sacs in Reactor Modelling. *Chemical Engineering Science* **1988**, *43(8)*, 1725-1738.

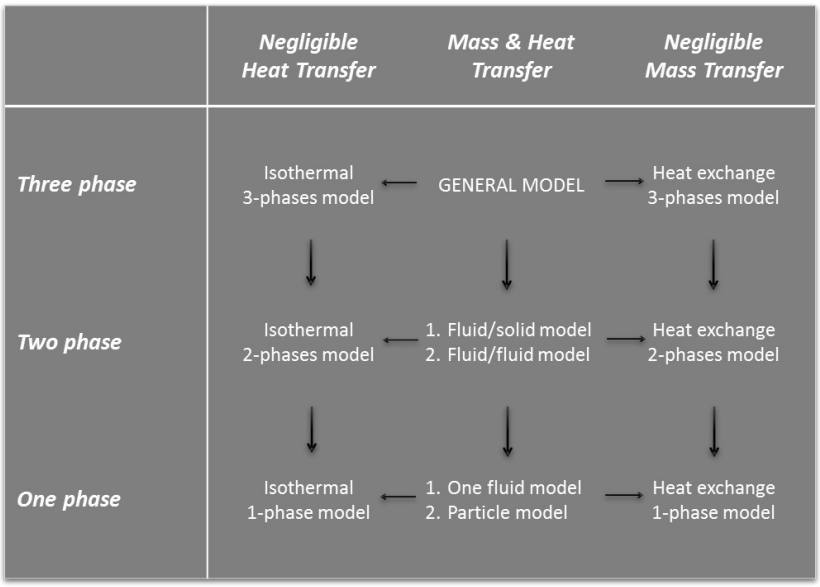

Figure 1 – Switchable continuous tubular reactor model.

The developed models were tested by parameter analysis and applying them to real cases of interest, describing experimental data collected in laboratory-scale equipment.

In particular, **Chapter 2** is dedicated to the description of the general heat exchanged three-phase model. A sugar hydrogenation process, namely hydrogenation of arabinose was selected as a case study, illustrating also the importance of catalyst deactivation in continuous reactors. The results can be found in **Publication II**, while a rationalization of the approach is presented in **Publication I**. An effort was made to model the behavior of microreactors, selecting the ethylene oxidation to ethylene oxide as a case study (**Chapter 3**). Two different models were developed, depending on the microreactor structure: (i) a washcoated microreactor, in which the reactions take place inside the coated catalyst layer; (ii) a silver-plate microreactor, where the reactor walls act as a catalyst. The results can be found in **Publication III**. **Chapter 4** was written to highlight the results obtainable with a two-phase sub-model, a packed bed reactor. The model was tested for ethanol partial oxidation on gold catalyst. The results were presented and analyzed in **Publication IV**.

A special case was devoted to the fluid-solid reactions, i.e. dissolution process, where the reactant is in solid phase and dissolves as a consequence of the reaction. A dedicated model was developed, namely shrinking particle-shrinking film model. The reaction proceeds both in the fluid film and bulk fluid. As a consequence, the particle becomes thinner, thus the surrounding film changes accordingly. Such model requires the solution of a moving boundary condition, i.e. the film thickness itself. This innovative approach is described in **Chapter 5**. The results of a parametric investigation and an application to a real case of interest (limestone dissolution in acidic environment) are shown. Further details can be found in **Publications V-VI**.

1.4 Applications and perspectives

The models presented in this thesis can find two possible applications. The short-term one in describing experiments collected in laboratory-scale reactors. By considering that the gPROMS Model Builder can be used to perform both parameter estimation and optimization activities, both kinetic and mass transfer studies can be conducted. A long-term application could be the design of large-scale reactors, such as packed bed and trickle bed reactors. Therefore, further improvement is needed to make the models even more general, such as considering the particle size distribution, or eventual particle aggregation and destruction phenomena for the shrinking-film models which could be described by taking into account population balances. Finally, the model could be used to describe experimental data collected from industrial scale systems. This would of course depend on the availability of these data and on the interaction between academia and chemical companies.

List of symbols

C_i	Concentration of component *i*, [mol/m^3]
$c_{p,i}$	Specific heat of component *i*, [J/(g·K)]
g	Gravitational acceleration constant, 9.822 [m/s^2]
H_i	Partial molar enthalpy, [J/mol]
J_i	Flux given by molecular diffusion, [mol/(m^3·s)]
M_i	Molecular weight of component *i*, [g/mol]
P	Pressure, [Pa]
Q_{rad}	Radiation heat flux, [J/(m^3·s)]
r_j	Reaction rate, [mol/(m^3·s)]
s	Shear stress, [Pa]
t	Time, [s]
T	Temperature, [K]
u	Fluid velocity, [m/s]

Greek symbols

ΔH_j	Reaction enthalpy of reaction *j*, [J/mol]
λ	Thermal conductivity, [J/(m·s·K)]
ρ_f	Fluid density, [kg/m^3]
$\nu_{i,j}$	Stoichiometric coefficient component *i* reaction *j*, [-]

Mathematical operators

∇	"Nabla" or "del" operator, expressing the gradient of a variable along its coordinates

Chapter 2 – Trickle bed reactor modelling: sugar hydrogenation

"There are no secrets to success. It is the result of preparation, hard work, learning from failure."

Colin Luther Powell, The Leadership Secrets of Colin Powell by Oren Harari, 2003

2.1 Introduction

The development of a general trickle bed reactor (TBR) model is the aim of the first part of this thesis. TBRs are one of the most used continuous heterogeneous catalytic reactors[20,21,22,23], where heterogeneously catalyzed gas-liquid reactions are carried out. They are used for several processes, e.g. ethanol oxidation to acetic acid[24], and hydrogenation reactions in petroleum industry[25].

Scaling-up TBRs requires more sophisticated models, solving both concentration and temperature profiles inside the reactor, at each location of the reactor and the catalyst particle[11,26]. In the present chapter, a modelling approach is described. The developed TBR modelling approach allows to obtain a simultaneous dynamic solution of the mass and energy balance equations, following in the footsteps of earlier TBR modelling studies[27,28]. The choice of a dynamic approach gives the model a good initialization and thereby to guarantee the convergence. Obviously, the power of such model characteristics is to simulate eventual catalyst deactivation, too.

The TBR model was applied on arabinose hydrogenation to arabitol as a case study. Starting from a known reaction kinetics, experiments performed in TBR were simulated, showing high performance of the model.

---

[20] L. Belfiore L. Transport Phenomena for Chemical Reactor Design. John Wiley& Sons, New Jersey: **2003**.

[21] J. Butt. Reaction Kinetics and Reactor Design. Marcel Dekker Inc., New York: **2000**.

[22] J. Hagen. Industrial Catalysis, A Practical Approach (2nd edition). Wiley-VCH Verlag GmpH, Weinheim: **1999**.

[23] V. Ranade, R.V. Chaudhari, P. Gunjal. Trickle-Bed Reactors–Reactor Engineering & Application. Elsevier, Amsterdam: **2011**.

[24] J. Klassen, R. S. Kirk. Kinetics of the Liquid-phase Oxidation of Ethanol. *AlChE J.* **1955**, *1(4)*, 488-495.

[25] C.N. Satterfield. Trickle-Bed Reactors. *AIChE J.* **1975**, *21(2)*, 209-228.

[26] F. Mederos, J. Ancheyta, J. Chen. Review on Criteria to Ensure Ideal Behaviours in Trickle-Bed Reactors. *Appl. Catal. A-Gen.* **2009**, *355*, 1-19.

[27] A. Iordanis. Mathematical Modelling of Catalytic Fixed Bed Reactors. Ph.D. Thesis. University of Twente (NL), **2002**.

[28] K. Metaxas, N. Papayannakos. Gas-Liquid Mass Transfer in a Bench-Scale Trickle Bed Reactor used for Benzene hydrogenation. *Chem. Eng. Tech.* **2008**, *31*, 410-417.

2.2 Trickle bed reactor model

For the trickle bed reactor model, the mass and heat balances for each phase (gas, liquid and solid) were solved simultaneously. The balances were time dependent, allowing the calculation of the concentration and temperature profiles inside each location of the reactor (axial and radial position) and inside the catalyst particles.

The dynamic mass balances of each component present in the gaseous and liquid phases are given in Eqs. 4-5,

$$\varepsilon_G \frac{\partial C_{i,G}}{\partial t} = -k_{i,L}a(C_i^* - C_{i,L}) - \frac{\partial u_G C_{i,G}}{\partial z} + \varepsilon_G D_{z,G}\frac{\partial^2 C_{i,G}}{\partial z^2} + \varepsilon_G D_{r,G}\left(\frac{\partial^2 C_{i,G}}{\partial r^2} + \frac{1}{r}\cdot\frac{\partial C_{i,G}}{\partial r}\right) \quad (4)$$

$$\begin{aligned}\varepsilon_L \frac{\partial C_{i,L}}{\partial t} = {} & +k_{i,L}a(C_i^* - C_{i,L}) - u_L\frac{\partial C_{i,L}}{\partial z} + \varepsilon_L D_{z,L}\frac{\partial^2 C_{i,L}}{\partial z^2} + \\ & + \varepsilon_L D_{r,L}\left(\frac{\partial^2 C_{i,L}}{\partial r^2} + \frac{1}{r}\cdot\frac{\partial C_{i,L}}{\partial r}\right) - \frac{D_{eff,i}s}{R_p}\frac{\partial C_{i,s}}{\partial r_p}\bigg|_{r_p=R_p}\end{aligned} \quad (5)$$

Both axial and radial dispersion terms are included in the balance equation. The concentration profiles are hence dependent on time as well as on the axial and radial location in the tubular reactor. As the reactions are assumed to proceed in the solid phase, the mass flux to and from the particles is introduced in the liquid balances. This kind of flux term has been earlier used for semi-batch cases[29,30].

The dynamic mass balance for each component present in the solid phase is shown in Eq. 6,

$$\frac{\partial C_{i,s}}{\partial t} = \frac{D_{eff,i}}{\varepsilon_p}\left(\frac{\partial^2 C_{i,s}}{\partial r_p^{\,2}} + \frac{s}{r_p}\frac{\partial C_{i,s}}{\partial r_p}\right) + \rho_s\sum\left(\nu_{i,j}r_j\frac{\varepsilon_L}{\varepsilon_p}\right) \quad (6)$$

[29] S. Toppinen, T. Rantakylä, T. Salmi, J. Aittamaa. Kinetics of the Liquid-Phase Hydrogenation of Benzene and Some Monosubstituted Alkylbenzenes over a Nickel Catalyst. *Ind. Eng. Chem. Res.* **1996**, *35*, 1824-1833.

[30] S. Toppinen, T. Rantakylä, T. Salmi, J. Aittamaa. Kinetics of the Liquid-Phase Hydrogenation of Di- and Trisubstituted Alkylbenzenes over a Nickel Catalyst. *Ind. Eng. Chem. Res.* **1996**, *35*, 4424-4433.

The concentration profiles of components (i) are solved at time t for a particle in the axial location (z), in the radial location (r) and inside the particle at the radial location (r_p). The shape factor (s) is evaluated by using Eq. 7[4,31] as a means for taking into account the particle geometry,

$$s+1=\left(R_p\frac{A_p}{V_p}\right) \tag{7}$$

The energy balances for the gas and liquid phases are reported in Eqs. 8-9,

$$\frac{\partial T_G}{\partial t}=-\frac{h_G a(T_G-T_L)}{\varepsilon_G\rho_G c_{p,G}}-\frac{\partial(u_G T_G)}{\partial z}+\left(\frac{\lambda_{z,G}}{\varepsilon_G\rho_G c_{p,G}}+D_{z,G}\right)\frac{\partial^2 T_G}{\partial z^2}+\left(\frac{\lambda_{r,G}}{\varepsilon_G\rho_G c_{p,G}}+D_{r,G}\right)\frac{1}{r}\frac{\partial T_G}{\partial r} \tag{8}$$
$$+\left(\frac{\lambda_{r,G}}{\varepsilon_G\rho_G c_{p,G}}+D_{r,G}\right)\frac{\partial^2 T_G}{\partial r^2}$$

$$\frac{\partial T_L}{\partial t}=+\frac{h_G a(T_G-T_L)}{\varepsilon_L\rho_L c_{p,L}}-u_L\frac{\partial T_L}{\partial z}+\left(\frac{\lambda_{z,L}}{\varepsilon_L\rho_L c_{p,L}}+D_{z,L}\right)\frac{\partial^2 T_L}{\partial z^2}+\left(\frac{\lambda_{r,L}}{\varepsilon_L\rho_L c_{p,L}}+D_{r,L}\right)\frac{1}{r}\frac{\partial T_L}{\partial r} \tag{9}$$
$$+\left(\frac{\lambda_{r,L}}{\varepsilon_L\rho_L c_{p,L}}+D_{r,L}\right)\frac{\partial^2 T_L}{\partial r^2}-\frac{\lambda_p s}{R_p\varepsilon_L\rho_L c_{p,L}}\cdot\left.\frac{\partial T_s}{\partial r_p}\right|_{r_p=R_p}$$

Convective heat flux, heat conduction to axial and radial directions, heat fluxes caused by axial and radial dispersion as well as heat flux from the particles are included in the model. Effective conductivities to the radial and axial direction of the reactor tube are assumed to be known to obtain realistic predictions. The liquid and the gas temperatures are solved along the time, the axial location (z) and the radial location (r).

The energy balance for the solid phase (Eq. 10) takes into account the heat conduction to the characteristic direction (r_p) and heat generation by reactions,

$$\frac{\partial T_s}{\partial t}=\frac{\lambda_p}{\rho_s c_{p,s}}\left(\frac{\partial^2 T_s}{\partial r_p{}^2}+\frac{s}{r_p}\frac{\partial T_s}{\partial r_p}\right)+\frac{1}{c_{p,s}}\frac{\varepsilon_L}{\varepsilon_p}\sum r_j(-\Delta H_r) \tag{10}$$

[31] R. Aris. On Shape Factors for Irregular Particles-I. The Steady-State Problem. Diffusion and Reaction. *Chem. Eng. Sci.* **1957**, *6*, 262-268.

In this case, the temperature profile is solved also along the particle radius coordinate.

The heat balance equation for the reactor jacket is given by as in Eq. 11,

$$\rho_J V_J c_{p,J} \frac{dT_J}{dt} = -u_J \rho_J V_J c_{p,J} \frac{dT_J}{dz} + UA_J \left(T_L\big|_{r=R_W} - T_J \right) \qquad (11)$$

In our case, the recirculating cooling liquid flow (u_J) and heat transfer coefficient (U) were set sufficiently high that the wall temperature remained constant.

The partial differential equation system (PDES) was solved numerically by using the numerical method of lines included in gPROMS ModelBuilder v. 3.7.1 software[32]. The method of lines is a numerical algorithm that leads to the solution of PDEs. It consists of the discretization of the spatial derivatives, leaving the time variable continuous. In this way, PDEs are transformed to a set of ordinary differential equations (ODEs)[33]. A number of different techniques fall within the method of lines family depending on the discretization method used for discretizing the spatial domain. Fixing the location of an element (x) inside the spatial domain, and fixing a spacing (h) given by the length of the domain divided by the number of discretization points, it is possible to define the discretization (δ) of a variable ($v(x)$) with different methods:

- Centered finite difference method: $\delta = v(x+0.5h) - v(x-0.5h)$;
- Backward finite difference method: $\delta = v(x) - v(x-h)$;
- Forward finite difference method: $\delta = v(x+h) - v(x)$;

In particular, radial derivatives were described with central difference approximation, while axial derivatives by backward difference approach. The selected grid of calculation points was: z=50, r=5, r_p=10 points.

[32] Process Systems Enterprise. gPROMS v3.7.1 User Guide, Process Systems Enterprise Ltd., London (U.K.), **2004**.
[33] W.E. Schiesser. The Numerical Method of Lines – Integration of Partial Differential Equations. Academic Press, New York: **1991**.

Solving the PDE system implies to define a proper set of initial and boundary conditions. In particular, the reactor was imagined to be filled with the feed concentration at t=0, at a constant temperature at the start-up.

The boundary conditions (BCs) were fixed as follows:

- z=0: feed concentrations and temperature
- z=L: axial derivatives of concentrations and temperature as zero (the Danckwerts' closed boundary condition)
- r=0: symmetry condition given by radial derivatives of concentration and temperature as zero
- r=R_W: concentration derivatives as zero and heat flux to the jacket
- r_p=0: symmetry given by zero-derivatives of both concentration and temperatures
- r_p=R_p: continuity equations being the solid wetted by the liquid.

Further details on the model and the calculation approach are reported in **Publications I** and **II**.

The TBR model is based on some general assumptions:

- Uniformity of the bed: this is obviously, the major ideality and approximation.
- At each location, mass and energy balances of each phase are solved, implying that for each point, the presence of all the three phases was assumed and heat convection, conduction and transfer were present. These assumptions smoothen inevitably the temperature gradients. Eventual hot spots generated by uneven packing, presence of stagnant liquid zones and liquid channeling cannot be seen in the results, because they are averaged away.
- For gas-liquid heat transfer, combined overall heat transfer coefficient h_{GA} was used, implying that the heat transfer did not count for local changes in the interfacial area, caused by unideal flow patterns or irregular shapes.
- The reactor wall considered well-wetted: in reality, the particles have different contact with the tube walls depending on their geometries.

The PDE system can be solved by fixing several necessary physical properties.

The form of the gas-liquid mass transfer coefficient was taken from Ellman correlation[11], corrected by an adjustable correction factor (γ), Eq. 12.

$$\frac{k_{A,L} a d_k^2}{D_{A,L}} = 0.45\gamma \left(X_G^{0.65} \, \mathrm{Re}_L^{1.04} \, We_L^{0.26} \, Sc_L^{0.65} \left(\frac{a_{sp} d_K}{1-\varepsilon_p} \right)^{0.25} \right)^{3.4} \tag{12}$$

It is well-known that the various gas-liquid mass transfer correlations reported in the literature give different results[28], thus the use of an adjustable parameter is inevitable.

According to our former experience with a laboratory-scale TBR, the order of magnitude value for Péclet number of the liquid phase was around 10, while plug-low behavior was assumed for the gas phase (*Pe*=100). Axial and radial dispersion coefficients were calculated from Eqs. 13-14, starting from the definition of the Péclet number. Radial dispersion is generally smaller than the axial dispersion (about three times).

$$D_{z,j} = \frac{u_j L}{Pe_j}, \; j = L, G \tag{13}$$

$$D_{r,j} = \frac{1}{3} D_{z,j}, \; j = L, G \tag{14}$$

The liquid hold-up was calculated from Eq. 15[34], correlating it as a function of the superficial liquid and gas velocities,

$$\varepsilon_L = k_\varepsilon u_L^{\,a_\varepsilon} u_G^{\,b_\varepsilon} \tag{15}$$

It was demonstrated that the liquid hold-up at very low superficial velocities is a weak function of the liquid Reynolds number and

[34] R. Lange, M. Schubert, T. Bauer. Liquid Hold-up in Trickle Bed Reactors at Very Low Liquid Reynolds Numbers. *Ind. Eng. Chem. Res.* **2005**, *44*, 6504-6508.

practically independent of the gas-phase Reynolds number, becoming therefore almost constant. An average value of 0.3 was obtained.

The axial pressure drop was calculated taking into the net flow direction that was downward, by implementing the friction factor[11] according to Eqs. 16 and 17.

$$f = \frac{1}{\left(X_G\left(\mathrm{Re}_L We_L\right)^{1/4}\right)^{3/2}}\left[31.3 + \frac{17.3}{\sqrt{X_G\left(\mathrm{Re}_L We_L\right)^{1/4}}}\right] \quad (16)$$

$$P = P_{IN} - 2zfd_K\rho_G u_G^2 \quad (17)$$

Assuming an axial pressure drop is certainly an approximation. As a matter of fact, it should be calculated by using momentum balance equations. We decided however to describe the flow related phenomena by backmixing, hold-up and pressure drop with semi-empirical expressions. This approach is a good approximation considering that in the actual case, the system was composed by a short reactor with a negligible pressure drop.

The heat conductivities of the particles were calculated by averaging the related internal liquid and solid conductivities, Eq. 18[35].

$$\lambda_p = \lambda_L(\lambda_S/\lambda_L)^{(1-\varepsilon_P)} = \lambda_L{}^{\varepsilon_P}\lambda_S{}^{1-\varepsilon_P} \quad (18)$$

This approximation is acceptable, even if it does not take into account the shape irregularities of the particle pores.

Concerning the phase partition, under the studied operating conditions (403K and 2MPa) arabinose and arabitol are present only in the liquid and solid phases, while hydrogen is present in all three phases. Thus, it is necessary to define the hydrogen solubility in the liquid phase, calculated from Eq. 19[36], where the reference value at $30\cdot10^5$Pa is used,

[35] Z.I.Önsan, A.K. Avci. Multiphase Catalytic Reactors: Theory, Design, Manufacturing, and Applications. Wiley, New Jersey: **2016**.
[36] V.A. Sifontes Herrera. Hydrogenation of L-Arabinose, D-galactose, D-Maltose and L-Rhamnose. Ph.D. Thesis. Åbo Akademi University (FI), **2012**.

$$C^*_{H_2} = C^*_{H_2,ref} \frac{P}{P_{ref}} \quad (19)$$

The liquid viscosity depends on both temperature and composition. It was calculated by implementing Eq. 20[36,37].

$$\eta_L = \exp\left(\frac{1.54 x_A}{T_L - 273} + 3.81 \cdot 10^{-4} x_A^{\,2} - 1.10 \cdot 10^{-2} x_A - 2.85 + \frac{1.94 \cdot 10^2}{T_L - 273} - \frac{3.89 \cdot 10^3}{(T_L - 273)^2} \right) \cdot 10^{-3} \quad (20)$$

Molecular diffusivities were calculated by applying the Wilke-Chang correlation[38], while the effective diffusivity was obtained by scaling the molecular diffusivities by particle porosity and tortuosity (Eq. 21), which is the parallel-pore model[35].

$$D_{eff,i} = D_i \frac{\varepsilon_p}{\tau} \quad (21)$$

The other necessary physical properties were considered constant with the actual pressure and temperature intervals. Average values at 403K are reported in Table 2.

Table 2 – List of the chemical/physical properties at 403 K.

Parameter	Value	Unit	Parameter	Value	Unit
ρ_L	950	kg/m^3	$D_{A,L}$	$4.0 \cdot 10^{-8}$	m^2/s
ρ_G	3.0	kg/m^3	$D_{B,L}$	$4.0 \cdot 10^{-8}$	m^2/s
ρ_{cat}	0.424	kg/m^3	$D_{H2,L}$	$1.9 \cdot 10^{-7}$	m^2/s
$c_{p,L}$	4300	J/(kg·K)	ΔH_r	$-82.0 \cdot 10^3$	J/mol
$c_{p,p}$	3000	J/(kg·K)	σ_L	$7.3 \cdot 10^{-4}$	N/m
$C_{H2,ref}^*$	25.0	mol/m^3	η_L	$0.2 \cdot 10^{-3}$	Pa·s

The catalyst effectiveness factor was calculated from the local reaction rates, Eq. 22[4].

[37] V.A. Sifontes Herrera, D.E. Rivero Mendoza, A.-R. Leino, J.-P. Mikkola, A. Zolotukhin, K. Eränen, T. Salmi. Sugar Hydrogenation in Continuous Reactors: From Catalyst Particles Towards Structured Catalysts. *Chemical Engineering and Processing: Process Intensification* **2016**, *109*, 1-10.

[38] C.R. Wilke, P. Chang. Correlation of Diffusion Coefficients in Dilute Solutions. *AICHE J.* **1955**, *1(2)*, 264-270.

$$\eta = \frac{\int_0^{Rp} r_j \cdot r_p^{s-1} \; dr_p}{r_j\big|_{r_p=R_p} \cdot \int_0^{Rp} r_p^{s-1} \; dr_p} \tag{22}$$

Another important aspect to be taken into account for the experiments performed in the TBR, is the catalyst deactivation observed during time-on-stream. The reaction rate was adjusted by a deactivation factor (α), given by a semi-empirical expression, in which the catalyst deactivation is assumed to originate from the organic reactant (Eq. 23),

$$-\frac{d\alpha}{dt} = (\alpha - \alpha^*) k_D \frac{C_{A,L}}{\left(1 + K_A C_{A,L} + K_{H2} C_{H2,L} + K_B C_{B,L}\right)^2} \tag{23}$$

Finally, all the fixed parameters for the TBR simulations are reported in Table 3. Operation conditions, reactor and particle dimensions and the initial conditions are included.

Table 3 – List of all properties characterizing the TBR simulations: mass and heat transfer, reactor, fluid, catalyst properties and initial conditions.

Mass and heat transfer			Reactor and catalyst			Initial conditions for each phase		
Pe_L	10	-	L	$3\cdot10^{-2}$	m	u_L	$2.6\cdot10^{-4}$	m/s
Pe_G	100	-	R_W	$5\cdot10^{-3}$	m	u_G	$4.2\cdot10^{-2}$	m/s
$\lambda_{r,L} = \lambda_{z,L}$	2	W/(m·K)	R_P	$1\cdot10^{-4}$	m	$C_{A,G}$	0	mol/m^3
$\lambda_{r,G} = \lambda_{z,G}$	0.1	W/(m·K)	w_{cat}	$1\cdot10^{-3}$	kg	$C_{A,L} = C_{A,S}$	$1\cdot10^{3}$	mol/m^3
λ_p	0.5	W/(m·K)	f_{active}	0.7	wt.%Ru	$C_{B,G} = C_{B,L} = C_{B,S}$	0	mol/m^3
k_ε	0.98	-	ε_G	0.3	-	$C_{H2,G}$	$6\cdot10^{2}$	mol/m^3
a_ε	0.14	-	ε_L	0.3	-	$C_{H2,L} = C_{H2,S}$	16	mol/m^3
b_ε	0.01	-	ε_P	0.4	-	$T_L = T_S = T_J$	403	K
T_w	403	K	s	2	-	T_G	363	K

2.3 Intrinsic kinetics of arabinose hydrogenation

Three-phase hydrogenation of arabinose to arabitol on ruthenium catalyst was chosen as a case study to test the TBR model. Experimental data were obtained from literature[39,40]. Experiments have been performed in a $1.2 \cdot 10^{-4}$ m^3 semi-batch reactor, using a 2.5 wt.% Ru on active carbon catalyst in powder form, by varying the temperature (363-403K), the hydrogen partial pressure ($4\text{-}6 \cdot 10^6$Pa) and the catalyst amount (0.5-0.1g). The rate expression was imposed, by considering that the reaction mechanism follows a Langmuir-Hinshelwood mechanism, Eq. 24, including a correction factor (α) for catalyst deactivation,

$$r_j = \frac{\alpha k \rho_{CAT} K_A K_{H_2} C_{A,S} C_{H_2,S}}{(1 + K_A C_{A,S} + K_{H_2} C_{H_2,S})^2} \tag{24}$$

In the case of batch experiments, no catalyst deactivation was observed. A parameter estimation activity was performed on the experimental data. The results were satisfactory, obtaining for each experiment a coefficient of determination value exceeding R^2=0.95. The kinetic parameters are reported in Table 4, along with the related statistical information, while an overall parity plot is displayed in Figure 2.

The estimated parameters are characterized by a low error and very low correlation. As it is revealed by the parity plot, a good agreement between the experimental and simulated values is obtained. Almost all data are inside a window of error of about ±10%. Further details on the obtained fits can be found in **Publication II**.

The kinetic rate equation, with the related parameters, was then directly used for the TBR experiments interpretation.

[39] V.A. Sifontes Herrera, O. Oladele, K. Kordás, K. Eränen, J.-P. Mikkola, D.Yu. Murzin, T. Salmi. Sugar Hydrogenation Over a Ru/C Catalyst. *J. Chem. Technol. Biotechnol.* **2011**, *86*, 658-668.
[40] D. Durante. Modeling of a Trickle Bed Reactor for L-Arabinose Hydrogenation. Master's Thesis. Åbo Akademi University (FI), **2011**.

Table 4 – Parameter estimation results for the arabinose hydrogenation experiments conducted in a semi-batch reactor. Reference temperature set at 403K. Confidence intervals and correlation matrix are included.

Parameter	Value	95% Confidence Interval
E_a [J/mol]	$6.45 \cdot 10^{4}$	$1.45 \cdot 10^{-1}$
K_A [m^3/mol]	$8.56 \cdot 10^{-4}$	$4.84 \cdot 10^{-9}$
K_{H2} [m^3/mol]	$5.95 \cdot 10^{-3}$	$1.76 \cdot 10^{-7}$
k_{ref} [mol/(g_{cat}·s)]	$6.34 \cdot 10^{-1}$	$1.47 \cdot 10^{-5}$

Correlation Matrix

	E_a	K_A	K_{H2}	k_{ref}
E_a	1.00			
K_A	0.01	1.00		
K_{H2}	0.68	0.50	1.00	
k_{ref}	-0.58	-0.66	-0.09	1.00

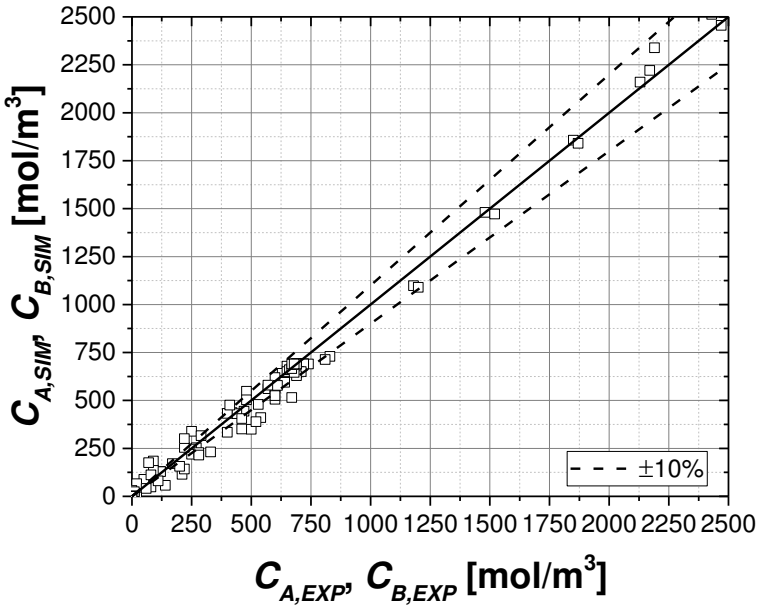

Figure 2 – Overall parity plot obtained for the parameter estimation activity on the arabinose hydrogenation kinetic experiments performed in a semi-batch reactor.

2.4 Arabinose hydrogenation in trickle bed reactor

The trickle bed reactor model was used to simulate arabinose hydrogenation experiments where catalyst deactivation was profound. Experimental data were obtained from literature[39]. The TBR properties and the experimental conditions are reported in Table 3.

In this case, the activity correction factor (α) starts from 1 and gradually decreases as a function of time, reaching a constant limit value, with a rate proportional to the deactivation rate constant (k_D). Our approach to catalyst deactivation implies that eventual plugging of the pores does not lead to a change in the effective diffusivity. The two phenomena (plugging and restricted access to sites) are correlated and difficult to be separated, but most probably both take place simultaneously. It was decided to adjust only the reaction rate by means of the activity correction, leaving the effective diffusivity invariant. It has to be reminded that the adjustable parameter for the gas-liquid mass transfer coefficient (γ) has to be estimated from the experimental data.

The results of the parameter estimation activities are collected in Table 5 and in Figure 3, where the obtained parameters and the arabinose conversion vs time-on-stream data are reported.

Table 5 – Parameter estimation results for the arabinose hydrogenation experiment performed in the trickle bed reactor. Confidence intervals and correlation matrix are included.

Parameter	**Value**	**95% Confidence Interval**
γ	$2.03 \cdot 10^{-2}$	$2.87 \cdot 10^{-5}$
α^*	$1.74 \cdot 10^{-4}$	$5.56 \cdot 10^{-7}$
k_D	$1.59 \cdot 10^{-5}$	$2.17 \cdot 10^{-8}$

Correlation Matrix

	γ	α^*	k_D
γ	1.00		
α^*	-0.20	1.00	
k_D	0.47	0.20	1.00

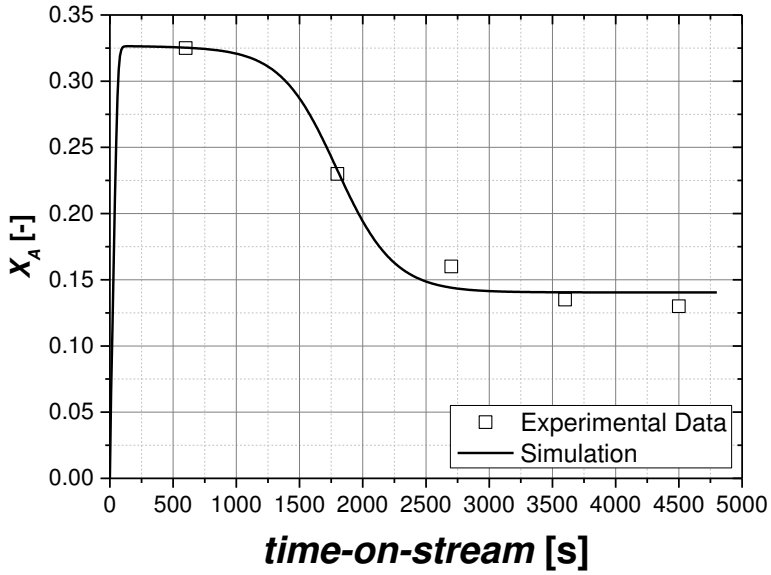

Figure 3 – Arabinose conversion vs time-on-stream for arabinose hydrogenation performed in TBR.

It can be concluded that the data were correctly reproduced with numerical simulations of the TBR model. The estimated gas-liquid mass transfer coefficient ($k_{A,L}a$) is in agreement with numerical values reported in literature[28]. The obtained parameters are only small correlated and the related confidence intervals are reliable.

2.5 Trickle bed reactor sensitivity study

A sensitivity study was carried out by using the TBR model, fixing the parameter estimated as in the previous sections. Because the model is four-dimensional (time, pipe axial and radial coordinates, particle radius), the results of each simulation are characterized by multi-dimensional matrices. Thus, it is not possible to plot directly the evolution of a variable along each coordinate. Therefore, the output was parametrized depending on the variable to be plotted.

As an example, in Figure 4, the arabinose conversion and the liquid temperature are plotted vs the TBR length and radius, by fixing the time at 1500 s.

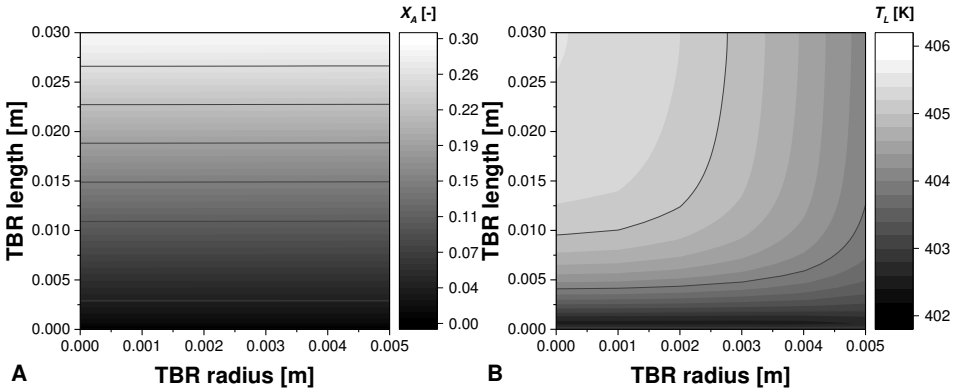

Figure 4 – A. Arabinose conversion contour plot vs TBR length and radius, at 1500 s. B. Liquid temperature profile at 1500 s as a function of TBR length and radius.

At the selected time, the arabinose conversion trend is quite linear along the TBR length and no radial gradients can be observed. Concerning the liquid temperature profile, it is evident that the liquid is first cooled by the gas, after which its temperature increases due to the heat released by the reaction. In this case, radial gradients of 2-3°C were observed due to the heat exchange to the jacket.

As the liquid is cooled by the gas, the gas phase is heated by the liquid phase as well. Coherent results were obtained for the concentrations and

temperature profiles inside the particle. As an example, in Figure 5A, simulation results are reported for a particle located in the middle of the TBR at 1500 s.

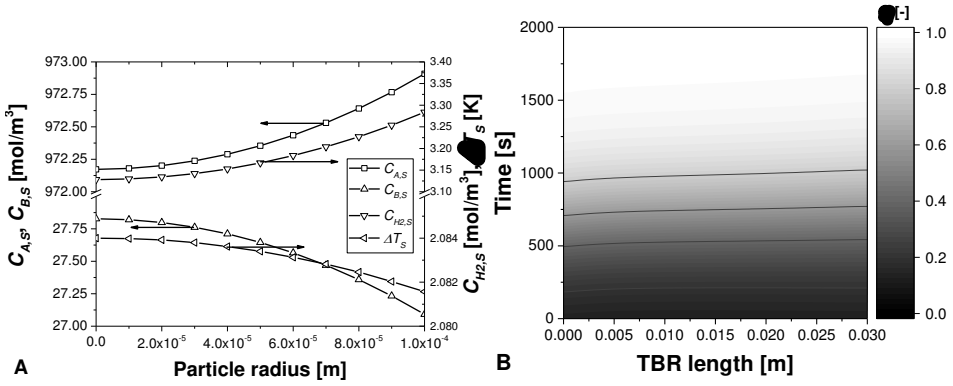

Figure 5 – A. Concentrations and temperature profiles along the particle radius, for a catalyst sphere located in the middle of the TBR, at 1500 s. B. Effectiveness factor trend vs the TBR axial coordinate and time, at r=0.

As expected, the concentrations of both reactants, arabinose and hydrogen, are decreasing along the particle radius, while the concentration of the product, arabitol, is increasing. As the reaction is exothermic, a temperature increase is observed inside the particle. The related gradient was very low because the catalyst had a small diameter. In Figure 5B, the effectiveness factor trend as a function of time and the TBR length coordinate is reported, fixing the radial coordinate at zero. The effectiveness factor increased with time and smoothly increased with the reactor length. The related increase was due to the decrease of the reaction rate caused by catalyst deactivation.

A high potential of the developed TBR model in predicting multiphase systems was demonstrated. Further simulations are reported in **Publication II**, highlighting the influence of other parameters (i.e. reactor length, axial dispersion, particle size) on the reaction rate, demonstrating its flexibility in predicting the behavior of laboratory-scale pilot plant reactors.

2.6 Conclusions

A comprehensive dynamic non-isothermal TBR model, for a multiphase gas-liquid-solid system was developed in this part of the thesis. The model can be considered to be a rather general one, including aspects which are crucially important for the simulation of trickle bed reactors in laboratory and industrial scale.

The selective three-phase hydrogenation of arabinose to arabitol was chosen as a case study. The intrinsic kinetics was investigated on specific experiments performed in a semi-batch reactor, while the deactivation factors and the gas-liquid mass transfer coefficient were obtained by parameter estimation analysis of a laboratory-scale TBR experiment.

The model was able to correctly describe the experimental data, showing a high flexibility.

List of symbols

A	Arabinose
A_J	Heat exchange surface area, [m^2]
A_P	Particle surface area, [m^2]
a_{sp}	Catalyst specific surface area, [m^2/m^3]
a_ε	Liquid void fraction parameter, [-]
B	Arabitol
b_ε	Liquid void fraction parameter, [-]
cat	Catalyst
C_i^*	Component i saturation concentration, [mol/m^3]
$C_{i,ref}^*$	Component i saturation concentration at reference pressure, [mol/m^3]
$C_{i,j}$	Concentration of component i in phase j, [mol/m^3]
$c_{p,j}$	Specific heat of phase j, [J/(kg·K)]
$c_{p,J}$	Specific heat of the jacket fluid, [J/(kg·K)]
$D_{eff,i}$	Effective diffusivity of component i in water, [m^2/s]
$D_{i,j}$	Molecular diffusivity of i in phase j, [m^2/s]
$D_{r,j}$	Radial dispersion coefficient of phase j, [m^2/s]
$D_{z,j}$	Axial dispersion coefficient of phase j, [m^2/s]
d_K	Krischer-Kast hydraulic diameter, [m], $d_P \sqrt[3]{\frac{16\varepsilon^3}{9\pi(1-\varepsilon)^2}}$
E_a	Activation energy, [J/mol]
f	Friction factor, [-]
f_{active}	Active phase (of ruthenium), [-]
H_2	Hydrogen
h	Spacing=length of the domain/number of discretization points
$h_{GL}a$	Gas-liquid heat transfer coefficient, [$W/(m^3·K)$]
i	Component i =A (arabinose), B (arabitol), H_2 (hydrogen)
j	Phase j = G (gas), L (liquid), p (particle)
k	Kinetic constant, [$mol/(g_{cat}·s)$]
K_A	Arabinose adsorption parameter, [m^3/mol]
K_B	Arabitol adsorption parameter, [m^3/mol]
k_D	Catalyst deactivation rate constant, [-]

K_{H2}	Hydrogen adsorption parameters, [m^3/mol]
$k_{i,L}a$	Gas liquid mass transfer coefficient for *i*, [s^{-1}]
k_{ref}	Kinetic constant at reference temperature, [mol/(g_{cat}·s)]
k_ε	Liquid void fraction parameter, [-]
L	Reactor length, [m]
P	Pressure, [Pa]
Pe_j	Péclet number of the phase *j*, [-] $Pe = d_P u_j / D_{i,j}$
P_{IN}	Initial pressure, [Pa]
P_{ref}	Reference pressure, [$30 \cdot 10^5$ Pa]
r	Radial location, [m]
R_W	Reactor radius, [m]
Re_L	Reynolds number for the liquid phase, [-], $\mathrm{Re}_L = \rho_L u_L d_P / \eta_L$
r_j	Reaction *j* rate, [mol/(g·s)]
r_p	Particle radial location, [m]
R_p	Particle radius, [m]
s	Shape factor, [-]
Sc_L	Schmidt number for the liquid phase, [-] $Sc = \eta_L / \rho_L d_P$
t	Time, [s]
T_j	Temperature of phase *j*, [K]
T_J	Jacket temperature, [K]
T_w	Wall temperature, [K]
U	Overall heat transfer coefficient, [W/(m^2·K)]
u_j	Velocity of the phase *j*, [m/s]
u_J	Velocity of the jacket fluid, [m/s]
v	Variable
V_J	Jacket volume, [m^3]
V_P	Particle volume, [m^3]
w_{cat}	Catalyst mass, [kg]
We_L	Weber number for the liquid phase, [-], $We_L = \rho_L u_L d_p / \sigma_L$
x	Location of an element inside the discretization domain, [-]
x_A	Arabinose initial concentration, [wt.%]
X_A	Arabinose conversion, [-]

X_G	Modified Lockhart-Martinelli ratio, [-] $X_G = (u_G / u_L)\sqrt{\rho_G / \rho_L}$
z	Axial location, [m]

Greek symbols

α	Catalyst deactivation factor, [-]
α^*	Final catalyst deactivation factor, [-]
γ	Ellmann correlation, adjustable parameter, [-]
δ	Discretization
ΔH_r	Reaction enthalpy, [J/mol]
ΔT_s	Particle surface-internal temperature difference, [K]
ε_j	Holdup of phase *j*, [-]
η	Effectiveness factor, [-]
η_j	Viscosity of phase *j*, [Pa·s]
λ_L	Fluid heat conductivity, [W/(m·K)]
λ_p	Particle heat conductivity, [W/(m·K)]
$\lambda_{r,j}$	Radial heat conductivity of the phase *j*, [W/(m·K)]
λ_S	Solid heat conductivity, [W/(m·K)]
$\lambda_{z,j}$	Axial heat conductivity of the phase *j*, [W/(m·K)]
ρ_j	Density of phase *j*, [kg/m^3]
ρ_J	Density of the jacket fluid, [kg/m^3]
ρ_{cat}	Catalyst concentration referred to liquid phase, [kg/m^3]
σ_L	Liquid surface tension, [N/m]
$\nu_{i,j}$	Stoichiometric coefficient for component *i* in phase *j*, [-]
τ	Particle tortuosity, [-]
χ	Dimensionless axial direction, [-]

Chapter 3 – Microreactor modelling: ethylene oxide synthesis

"The fundamental laws necessary for the mathematical treatment […] chemistry are thus completely known, and the difficulty lies only in the fact that application of these laws leads to equations that are too complex to be solved."

Paul Dirac, Proceedings of the Royal Society, 1929

3.1 Introduction

The development of microreactor models is the topic of the present chapter. These kinds of reactors are gaining high interest in chemical engineering, because of many reasons, i.e. (i) investigation of the intrinsic kinetics of rapid reactions, (ii) process intensification, (iii) suppression of heat and mass transfer limitations, (iv) operation under safe conditions.

In particular, microreactors allow investigate the kinetics of rapid reactions, fact mainly due to two intrinsic properties: the washcoated catalyst layers in micro-channels are typically very thin (20-40μm) and the related mass and heat transfer characteristics are excellent. In this way, eventual internal mass transfer resistance has less impact on the overall rate of the process and it is possible to work under isothermal conditions even with exothermic reactions. Thus, gas-phase microreactors are usually modelled as ideal reactors, characterized by low residence times and a plug-flow behavior[41].

Modelling a microchannel is very similar to modelling a monolithic reactor, i.e. when operating with diluted streams or when the microreactors are constructed of highly conductive materials. In these cases, the axial heat conduction resistance in the solid reactor wall can be neglected, considering the system to be isothermal. Models for reactors both with and without a washcoat have been already developed for gas-solid systems[42,43,44]. For this reason, an effort in rationalizing a comprehensive microreactor model was made in this part of the thesis.

Ethylene oxide synthesis was selected as a model system, being a highly exothermic gas phase reaction catalyzed by heterogeneous catalysts. As a matter of fact, our group published a paper where a huge number of experiments were conducted in both washcoated and silver-plate

[41] V. Hessel, S. Hardt, H. Löwe. Chemical Micro Process Engineering. Wiley-VCH, Weinheim: **2004**.
[42] M. Stutz, D. Poulikakos. Optimum Washcoat Thickness of a Monolith Reactor for Syngas Production by Partial Oxidation of Methane. *Chem. Eng. Sci.* **2008**, *63*, 1761-1770.
[43] O. Deutchmann, R. Schwiedernoch, L. Maier, D. Chatterjee. Natural Gas Conversion in Monolithic Catalysts: Interaction of Chemical Reactions and Transport Phenomena. *Stud. Surf. Sci. Catal.* **2001**, *136*, 251-258.
[44] A. Pattegar, M. Kothare. A Microreactor For Hydrogen Production in Micro Fuel Cell Applications. *J. Microelectromech. S.* **2004**, *13*, 7-11.

microreactors. The preliminary data interpretations were far from being satisfactory[45]. An important issue that could explain this lack of agreement is the role of the internal mass transfer resistance in the pores of the washcoat layer. Even if the coating is thin, the reaction rate can be retarded by diffusion limitations, if the kinetic process itself is rapid, as it has recently been illustrated[46]. It will be demonstrated that by describing the experimental data with this new approach, it is possible to correctly interpret all experimental data.

3.2 Microreactor modelling

Two kinds of microreactors were used for ethylene oxidation to ethylene oxide, i.e. a washcoated microreactor, where the active phase is Ag/Al_2O_3, and a silver plate microreactor. In the first case, the reactions and internal diffusion of each compound inside the catalyst layer were included, while in the second case the reaction was considered to take place on the channel walls only (Figure 6).

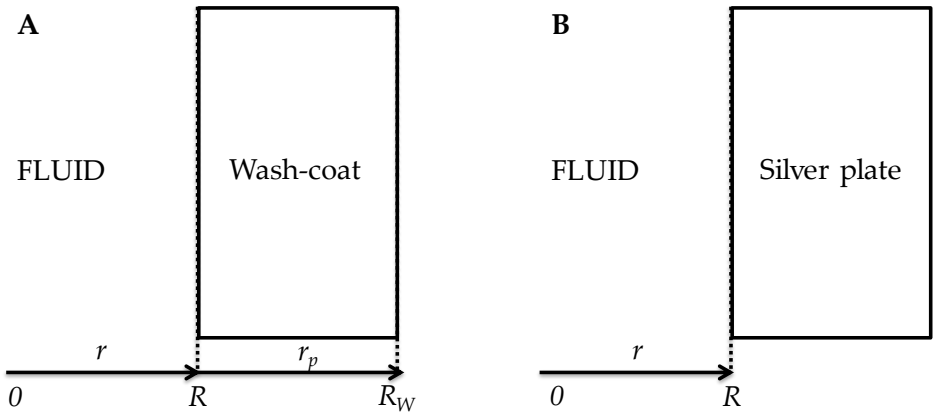

Figure 6 – Microreactor models: A. washcoated; B. silver plate.

[45] J. Carucci, V. Halonen, K. Eränen, J. Wärnå, S. Ojala, M. Huuhtanen, R. Keiski, T. Salmi. Ethylene Oxide Formation in A Microreactor: From Qualitative Kinetics to Detailed Modelling. *Ind. Eng. Chem. Res.* **2010**, *49*, 10897-10907.

[46] S.A. Schmidt, N. Kumar, A. Reinsdorf, K. Eränen, J. Wärnå, D. Murzin, T. Salmi. Methyl Chloride Synthesis on Al_2O_3 in a Microstructured Reactor – Thermodynamics, Kinetics and Mass Transfer. *Chem. Eng. Sci.* **2013**, *95*, 232-245.

The developed models are dynamic, based on radial and axial dispersion. Because the experiments were performed under isothermal conditions, energy balances were not included.

The model for the washcoated microreactor consists of two sets of PDEs, representing the fluid and the solid mass balance equations, Eqs. 25-26.

$$\frac{\partial C_{i,F}}{\partial t} = -u_F \frac{\partial C_{i,F}}{\partial z} + D_{z,F} \frac{\partial^2 C_{i,F}}{\partial z^2} + D_{r,F}\left(\frac{\partial^2 C_{i,F}}{\partial r^2} + \frac{1}{r}\frac{\partial C_{i,F}}{\partial r} \right) \tag{25}$$

$$\frac{\partial C_{i,s}}{\partial t} = \frac{D_{eff,i}}{\varepsilon_p}\left(\frac{\partial^2 C_{i,s}}{\partial r_p^{\,2}} + \frac{s}{r_p}\frac{\partial C_{i,s}}{\partial r_p} \right) + \frac{1}{\varepsilon_p}\sum\left(\nu_{i,j} r_j\right) \tag{26}$$

Convective and dispersion fluxes (both axial and radial) were included in the fluid phase mass balances, while reaction and internal diffusion terms were included in the mass balances for the washcoat layer.

The silver-plate microreactor model consists of one set of PDEs. As the reactions occur on the non-porous catalyst wall, it is necessary to write only one mass balance equation related to the fluid phase, Eq. 27.

$$\frac{\partial C_{i,F}}{\partial t} = -u_F \frac{\partial C_{i,F}}{\partial z} + D_{z,F} \frac{\partial^2 C_{i,F}}{\partial z^2} + D_{r,F}\left(\frac{\partial^2 C_{i,F}}{\partial r^2} + \frac{1}{r}\frac{\partial C_{i,F}}{\partial r} \right) + \sum\left(\nu_{i,j} r_j\big|_{r=R}\right) \tag{27}$$

Heat balance equations were tested, too, and flat temperature profiles were always obtained.

The reactor was assumed to be filled with the feed concentration at t=0. The boundary conditions (BCs) were fixed as follows,

- z=0: feed concentrations
- z=L: axial derivatives of concentrations and temperature are zero (Danckwerts' closed boundary condition)
- r=0: symmetry condition given by radial derivatives of concentration and temperature as zero
- r=R: continuity equation being the gas and the solid phases in contact (radial dispersion was not included):

$$u_F \left.\frac{\partial C_{i,F}}{\partial z}\right|_{r=R} = D_z\big|_{r=R} \frac{\partial^2 C_{i,F}}{\partial z^2} + \frac{D_{eff,i} s}{R_W - R} \left.\frac{\partial C_{i,S}}{\partial r_P}\right|_{r_P = R_W}$$

- $r=R_W$: zero derivative.

Further details of the model can be found in **Publication III**.

The PDE system was solved numerically by using the numerical method of lines built in gPROMS ModelBuilder v. 3.7.1 software[32]. In particular, radial derivatives are described with central differences, whereas axial derivatives are described by backward difference formula. The selected grid of calculation points was: z=50, r=10, r_p=10 points.

Several physical properties are needed in the calculations. The molecular diffusivities of each reactive component were calculated in helium (B), which was used for diluting the oxygen-ethylene mixture. The Wilke and Lee correlation[47], Eq. 28, was used.

$$D_{A,B} = \frac{\left[3.03 - (0.98/M_{AB}^{1/2})\right] \cdot T^{3/2} \cdot 10^{-3}}{P \cdot M_{AB}^{1/2} \cdot \sigma_{AB}^{2} \cdot \Omega_D} \tag{28}$$

The related parameters were calculated starting from known physical properties listed below:

$$M_{AB} = 2 \cdot \left[(1/M_A) + (1/M_B)\right]^{-1} \tag{29}$$

$$\sigma_{AB} = 1.18 \cdot (0.285 \cdot V_c^{1.048})^{1/3} \tag{30}$$

$$\Omega_D = \frac{1.06036}{(T^*)^{0.1561}} + \frac{0.193}{\exp(0.47635T^*)} + \frac{1.03587}{\exp(1.52996T^*)} + \frac{1.76474}{\exp(3.89411T^*)} \tag{31}$$

$$T^* = \frac{k \cdot T}{\varepsilon_{AB}} \tag{32}$$

$$\frac{\varepsilon_{AB}}{k} = 1.15 \cdot T_b \tag{33}$$

The effective diffusivities in the washcoat layer were considered to be 1/10 of molecular diffusivities, due to porosity and tortuosity correction, as suggested in literature[20].

[47] C.Y. Wilke, C.Y. Lee. Estimation of Diffusion Coefficients for Gases and Vapors. *Ind. Eng. Chem. Res.* **1955**, *47*, 1253-1257.

The washcoat thickness was 20 μm (from SEM images), while the porosity was in the range of 0.3-0.4.

The gas density depends strongly on the temperature. It was calculated from the ideal gas law by considering that for a 70% helium containing flow, an average molecular mass of 11g/mol can be assumed.

Finally, the axial dispersion coefficient was calculated by using an order of magnitude value of 100 for the gas-phase Péclet number, acceptable for low-dispersed flows, i.e. in the microreactor case[48],

$$D_{z,F} = \frac{u_F L}{Pe}, D_{r,F} = \frac{1}{3} D_{z,F} \qquad (34)$$

The radial dispersion coefficient value was taken as 1/3 of the axial dispersion coefficient. The sensitivity of the reaction system on radial dispersion was screened, by performing three simulations with 1/5, 1/10 and 1/15 times the axial dispersion. In every case, quite the same conversion was reached which implies that the heuristic value was reasonable.

[48] C.H. Hornung, M.R. Mackley. The measurement and characterization of residence time distributions for laminar liquid flow in plastic microcapillary arrays. *Chem. Eng. Sci.* **2009**, *64*, 3889-3902.

3.3 Ethylene oxide synthesis reaction mechanism

The reaction scheme for the partial oxidation of ethylene to ethylene oxide is shown in Figure 7, where the exothermic nature of the reactions is reported. The generally accepted view on the reaction mechanism is that ethylene epoxidation and total oxidation are essentially parallel processes[49]; thus, the role of reaction 3 in the scheme is minor compared to reactions 1 and 2.

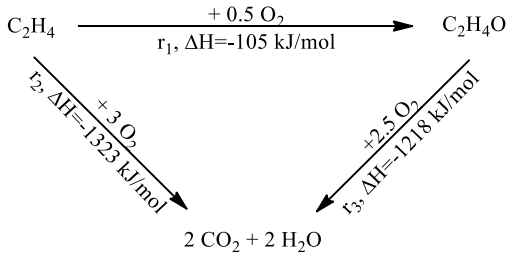

Figure 7 – Ethylene oxide synthesis from ethylene partial oxidation reaction path.

Several hypotheses have been proposed for explaining the reaction mechanism of ethylene oxidation on silver surfaces[45,49,50,51,52,53,54,55]. Initially it was proposed that molecularly adsorbed oxygen was responsible for selective reaction (r_1), while atomic surface oxygen caused nonselective reaction (r_2). Due to the stoichiometry of the resulting decomposition reaction ($7C_2H_4 + 6O_2 \rightarrow 6(C_2H_4)O + 2CO_2 + 2H_2O$), a maximum ethylene oxide selectivity of 6/7 (87.5%) should be reached, fact in contradiction with the higher selectivity observed in other works[49], indicating that a

[49] M.O. Özbek, R.A. van Santen. The Mechanism of Ethylene Epoxidation Catalysis. *Catal. Lett.* **2013**, *143*, 131-141.

[50] A. Kursawe. Partial Oxidation of Ethylene to Ethylene Oxide in Microchannel Reactors. PhD thesis. Technische Universität Chemnitz (D), **2009**.

[51] T. Salmi, J. Carucci, M. Roche, K. Eränen, J. Wärnå, D. Murzin. Microreactors As Tools in Kinetic Investigations: Ethylene Oxide Formation on Silver Catalyst. *Chem. Eng. Sci.* **2013**, *87*, 306-314.

[52] P. Borman, K. Westerterp. An experimental study of the kinetics of the selective oxidation of ethene over a silver on α-Al_2O_3 catalyst. *Ind. Eng. Chem. Res.* **1995**, *34*, 49-58.

[53] S. Ghazali, D. Park, G. Gasu. Kinetics of Ethylene Epoxidation on A Silver Catalyst. *Appl. Catal.* **1983**, *6*, 195-208.

[54] D. Lafarga, M Al-Joaied, C. Bondy, A. Varma. Ethylene Epoxidation on Ag-Cs/A-Al_2O_3 Catalyst: Experimental Results and Strategy for Kinetic Parameter Estimation. *Ind. Eng. Chem. Res.* **2000**, *39*, 2148-2156.

[55] L. Petrov, A. Eliyas, C. Maximov, D. Shopov. Ethylene Oxide Oxidation Over a Supported Silver Catalyst. *Appl. Catal.* **1988**, *41*, 23-38.

particular atomically adsorbed oxygen atom is responsible for the ethylene oxide selectivity.

In a recently published molecular modelling study based on Density Functional Theory (DFT) calculations, a common surface intermediate was proposed for the formation of ethylene oxide and carbon dioxide[49], that is an oxometallacycle intermediate giving either ethylene oxide or acetaldehyde that promptly decomposes to CO_2 and H_2O.

The following rate expression was used for ethylene epoxidation and total oxidation,

$$r_j = \frac{k_j C_E {C_{O_2}}^{\alpha_j}}{(1 + K_E C_E + K_{O_2} {C_{O_2}}^{\beta_j})^2} \qquad (35)$$

where j=1 and j=2 refer to epoxidation and total oxidation, respectively. In the adopted experimental conditions, the total oxidation according to reaction 3 can be excluded, as suggested in the literature[45].

The experimental observations collected previously in our laboratory indicated the following effective reaction orders: α_1=1, α_2=1/2, β_1=β_2=1[51]. For the sake of simplicity, the contribution of dissociatively adsorbed oxygen was ignored in the denominator of the equation, which implies that the dominating adsorption form of oxygen is molecular.

3.4 Microreactors modelling results

The developed microreactor models were used to interpret the experimental data published by Carucci et al.[45]. The authors performed an extensive kinetic investigation by varying different operation conditions: temperature, fluid velocity, ethylene-to-oxygen ratio. In the present work, two separated parameter estimation activities were conducted on the data collected by using different microreactors, wash-coated and silver plate.

Figure 8 shows the results obtained from parameter estimation performed for the experimental data collected in a washcoated microreactor. The estimated parameters, along with their statistic information, are listed in Table 6.

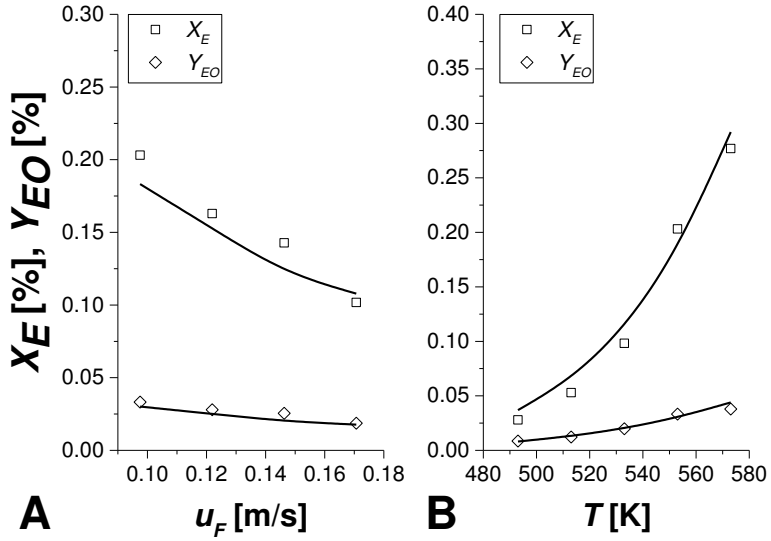

Figure 8 – Experimental results and related modelling using a washcoated microreactor for ethylene oxide synthesis, by imposing an ethylene/oxygen molar ratio of about 2. A. Influence of the fluid velocity (T=553K). B. Temperature influence (u_F=0.1 m/s).

Table 6 – Parameter estimation results obtained for the washcoat microreactor. The reference temperature was set at 553K.

Parameter	Value	95% Confidence Interval
$E_{a,1}$ [J/mol]	$4.59 \cdot 10^{4}$	$1.68 \cdot 10^{2}$
$E_{a,2}$ [J/mol]	$5.70 \cdot 10^{4}$	$1.73 \cdot 10^{2}$
$k_{1,ref}$ [m³/(mol·s)]	$4.98 \cdot 10^{-1}$	$3.62 \cdot 10^{-1}$
$k_{2,ref}$ [m³/(mol·s)]	$3.73 \cdot 10^{0}$	$2.71 \cdot 10^{0}$
K_E [m³/mol]	$4.10 \cdot 10^{0}$	$1.57 \cdot 10^{0}$
K_{O2} [m³/mol]	$3.16 \cdot 10^{-1}$	$2.43 \cdot 10^{-1}$

Correlation Matrix

	$E_{a,1}$	$E_{a,2}$	$k_{1,ref}$	$k_{2,ref}$	K_E	K_{O2}
$E_{a,1}$	1.00					
$E_{a,2}$	0.65	1.00				
$k_{1,ref}$	0.12	-0.01	1.00			
$k_{2,ref}$	0.01	0.15	0.25	1.00		
K_E	0.58	-0.58	0.42	-0.52	1.00	
K_{O2}	-0.60	-0.61	0.57	0.57	0.92	1.00

The success in performing simultaneous parameter estimation, being able to describe all the data, is the first promising result of this work. In a previously published paper by our group[45], a simple plug flow model was able to describe only results at a single temperature only. It is evident that such model is not adequate to describe the entire physics of the system. In our case, all the experiments were described together.

All the qualitative phenomena are well interpreted. For instance, at higher gas velocities, both ethylene conversion and ethylene oxide yield decreased. Moreover, at higher temperatures, an increase of the reaction rates is expected, thus both the main and side reactions become faster.

The numerical values of the parameters are physically reasonable. The activation energy values are in line with a strong dependence of the kinetic constant with temperature. The ethylene adsorption constant is ca. 10 times larger than that of oxygen. Therefore, these values are highly correlated, because they are not calibrated with specific experiments conducted by varying the feed composition.

A similar approach was followed in interpreting the kinetic experiments carried out in the pure silver-plate microreactor[45]. Simultaneous parameter estimation was successfully applied on a large number of experimental data (see details in **Publication III**). The results are reported in Figure 9 and in Table 7.

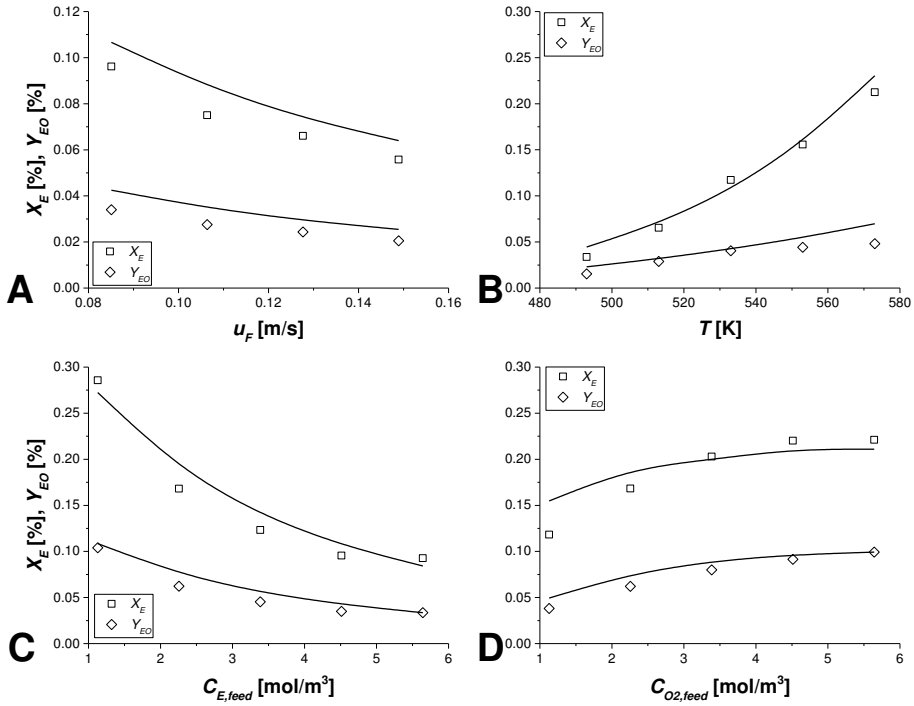

Figure 9 – Experimental results and related modelling using a silver-plate microreactor for ethylene oxide synthesis. A. Influence of the fluid velocity (T=553K, $C_{E,feed}/C_{O2,feed}$ =2mol/mol). B. Temperature influence (u_F=0.1 m/s, $C_{E,feed}/C_{O2,feed}$ =2mol/mol). C. Ethylene feed concentration influence (u_F=0.1 m/s, T=533K, $C_{O2,feed}$=2.26 mol/m^3). D. Oxygen feed concentration influence (u_F=0.1 m/s, T=533K, $C_{E2,feed}$=2.26 mol/m^3).

Table 7 – Parameter estimation results obtained for the silver-plate microreactor. The reference temperature was set at 553K.

Parameter	Value	95% Confidence Interval
$E_{a,1}$ [J/mol]	$3.10 \cdot 10^{4}$	$7.15 \cdot 10^{1}$
$E_{a,2}$ [J/mol]	$5.44 \cdot 10^{4}$	$9.05 \cdot 10^{1}$
$k_{1,ref}$ [m³/(mol·s)]	$1.54 \cdot 10^{-4}$	$2.55 \cdot 10^{-7}$
$k_{2,ref}$ [m³/(mol·s)]	$3.14 \cdot 10^{-4}$	$6.55 \cdot 10^{-7}$
K_E [m³/mol]	$3.59 \cdot 10^{-1}$	$7.35 \cdot 10^{-4}$
K_{O2} [m³/mol]	$2.69 \cdot 10^{-1}$	$6.62 \cdot 10^{-4}$

Correlation Matrix

	$E_{a,1}$	$E_{a,2}$	$k_{1,ref}$	$k_{2,ref}$	K_E	K_{O2}
$E_{a,1}$	1.00					
$E_{a,2}$	0.10	1.00				
$k_{1,ref}$	-0.09	0.02	1.00			
$k_{2,ref}$	0.01	0.08	0.02	1.00		
K_E	0.02	0.06	-0.03	-0.05	1.00	
K_{O2}	-0.06	-0.04	0.05	-0.06	0.05	1.00

Concerning the influence of temperature and gas velocity on the conversion of ethylene and selectivity of ethylene oxide, the results are similar to those obtained for the washcoated microreactor. By varying the feed composition, a strong variation of the reaction rates was observed. In particular, an increase in the ethylene feed concentration leads to a decrease of both ethylene conversion and ethylene oxide yield which can be explained by the ethylene inhibition. An opposite trend was observed by increasing the oxygen concentration: an apparent plateau was reached. It is evident that oxygen has a lower inhibition effect than ethylene on the silver surface. As a consequence, the ethylene adsorption constant is higher than the one for oxygen. These parameters are less correlated than for the washcoated case, because they are calibrated on experiments conducted at different reactant ratios, being therefore much more reliable.

3.5 Conclusions

Two different microreactor models were developed for the partial oxidation of ethylene to ethylene oxide, using washcoated and silver-plated microreactors; the first has a catalyst layer through which the reactants and products diffuse and react, while for the second one reaction occurs on the reactor wall. The models were written by treating the fluid dynamics in simple terms. The mass balance equations consisted of sets of partial differential equations, which were solved with a well-known method of lines.

Experimental data reported in the literature were described with the models and a good agreement with the data and the model predictions was achieved. The obtained results revealed that both models were capable of explaining all the collected experimental data.

We are confident that a tool to describe any fluid-solid microreactor system has been developed. This tool could be very useful in scale-up, or more punctually speaking, number-up microdevices in which highly exothermic and rapid reactions can be performed.

List of symbols

$C_{i,F}$	Concentration of component *i* in gas, [mol/m^3]
$C_{i,S}$	Local concentration of component *i* in solid, [mol/m^3]
C_E	Concentration of ethylene, [mol/m^3]
C_{O2}	Concentration of oxygen, [mol/m^3]
$C_{i,feed}$	Feed concentration of component *i*, [mol/m^3]
$D_{A,B}$	Diffusivity of compound *A* in *B*, [m^2/s]
$D_{eff,i}$	Effective diffusivity of component *I*, [m^2/s]
$D_{r,F}$	Radial dispersion coefficient, [m^2/s]
$D_{z,F}$	Axial dispersion coefficient, [m^2/s]
$E_{a,j}$	Activation energy of reaction *j*, [J/mol]
i	Component *i*
j	Reaction *j*
k	Parameter
k_j	Kinetic constant of reaction *j*, [(m^3/mol)^2·s^{-1})]
$k_{j,ref}$	Kinetic constant at reference temperature, [(m^3/mol)^2·s^{-1})]
K_E, K_{O2}	Adsorption constant for ethylene and oxygen, [m^3/mol]
L	Reactor length, [m]
M_A	Molecular mass solute, [g/mol]
M_B	Molecular mass of solvent, [g/mol]
M_{AB}	Mean molecular mass, [g/mol]
P	Pressure, [Pa]
Pe	Péclet number, [-]
R	Inner reactor radius, [m]
R_W	Reactor radius, [m]
r	Radial location, [m]
r_p	Radial location within the washcoat layer, [m]
r_j	Reaction rate expression of reaction *j*, [mol/(m^3·s)]
s	Shape factor, [-]
t	Time, [s]
T	Temperature, [K]
T^*	Boiling point, [K]
T_b	Boiling point, [K]
u_F	Superficial velocity of fluid (gas), [m/s]
V_c	Critical molar volume of component *i*, [cm^3/mol]
X_E	Conversion of ethylene, [%]
Y_{EO}	Yield, [%]

z	Axial location, [m]

Greek symbols

α, β	Parameters in rate equation, [-]
ΔH	Reaction enthalpy, [kJ/mol]
ε_p	Porosity, [-]
ε_{AB}	Parameter
$\nu_{i,j}$	Stoichiometric coefficient of component i in reaction, [-]
σ_{AB}	Parameter, [-]
Ω_D	Parameter, [-]

Chapter 4 – Packed bed reactor modelling: ethanol oxidation

"The three great essentials to achieve anything worthwhile are, first, hard work; second, stick-to-itiveness; third, common sense."

Thomas A. Edison, Men who made America great by Bertie Charles Forbes, 1917

4.1 Introduction

Packed bed reactors (PBR) are undoubtedly the most applied laboratory-scale reactor for heterogeneously catalyzed gas-phase processes, used both for catalyst screening and kinetic investigation and model verification. They are very often modeled by assuming a plug-flow fluid dynamics with negligible axial and radial dispersion effects. Most of the models presume steady state and neglect energy balance equations. Such models are fast-running, particularly well-suited for parameter estimation where an optimal solution is found by a large number of successive iterations. However, in some cases the obtained results are not reliable. Certain effects must be included, such as eventual fluid-solid mass transfer resistance[56].

In this part of the work, a dynamic general PBR model was developed, taking into account also the intraparticular diffusion effects in catalyst pores. The model was tested with a gas-solid reaction, partial oxidation of ethanol in the presence of gold nanoparticles as heterogeneous catalyst. Different kinetic expressions were screened and the results were compared.

4.2 Packed bed reactor model

The transient packed bed reactor model consists of a set of partial differential equations, given by the mass and energy balances for each phase. The mass balance for one component present in the gas phase is given in Eq. 36.

$$\varepsilon_G \frac{\partial C_{i,G}}{\partial t} = -\frac{\partial u_G C_{i,G}}{\partial z} + \varepsilon_G D_{z,G} \frac{\partial^2 C_{i,G}}{\partial z^2} + \varepsilon_G D_{r,G} \left(\frac{\partial^2 C_{i,G}}{\partial r^2} + \frac{1}{r} \frac{\partial C_{i,G}}{\partial r} \right) - N_{G,S,i} \quad (36)$$

[56] E. Santacesaria, R. Tesser, M. Di Serio, M. Guida, D. Gaetano, A. Garcia Agreda. Kinetics and Mass Transfer of Free Fatty Acids Esterification with Methanol in a Tubular Packed Bed Reactor: A Key Pretreatment in Biodiesel Production. *Ind. Eng. Chem. Res.* **2007**, *46*, 5113-5121.

The model is dynamic and both axial and radial dispersion effects are included. The net flux of a component *i* from the gas to the solid phase must be considered, given as by Eq. 37.

$$N_{G,S,i} = \frac{D_{eff,i} s}{R_p} \frac{\partial C_{i,S}}{\partial r_p}\bigg|_{r_p=R_p} \tag{37}$$

The mass balance for an arbitrary component *i* in the solid phase is defined in Eq. 38.

$$\frac{\partial C_{i,S}}{\partial t} = \frac{D_{eff,i}}{\varepsilon_S}\left(\frac{\partial^2 C_{i,s}}{\partial r_p^{\,2}} + \frac{s}{r_p}\frac{\partial C_{i,S}}{\partial r_p}\right) + \rho_S \frac{\varepsilon_G}{\varepsilon_S}\sum(v_{i,j} r_j) \tag{38}$$

The geometry of a particle can be taken into account by adjusting the shape factor value (*s*) given by

$$s + 1 = \left(R_p \frac{A_p}{V_p}\right) \tag{39}$$

The energy balance for the packed bed follows Eq. 40.

$$\frac{\partial T_B}{\partial t} = -\frac{\partial u_G T_B}{\partial z} + \frac{\lambda_{z,B}}{\rho_B C_{p,B}}\frac{\partial^2 T_B}{\partial z^2} + \frac{\lambda_{r,B}}{\rho_B C_{p,B}}\left(\frac{\partial^2 T_B}{\partial r^2} + \frac{1}{r}\frac{\partial T_B}{\partial r}\right) + \\ + \sum(-\Delta H_{r,j} r_j)/(\rho_B C_{p,B}) \tag{40}$$

In this case, a single energy balance equation was written for the entire bed, and a single temperature profile averaged for the two phases was calculated. Hence, axial and radial thermal conduction within the bed and the reaction heats of all reactions were included.

The partial differential equation system (PDE) was solved numerically by using the numerical method of lines included in gPROMS ModelBuilder v. 3.7.1 software[32]. Central difference approximations were

used with a grid of calculation points consisting of: z=20, r=5, r_p=10 points.

For solving the PDE system, an appropriate set of initial and boundary conditions should be defined. In particular, the reactor was imagined to be filled with the feed concentration at t=0, at a constant temperature.
The boundary conditions (BCs) were fixed as follows:

- z=0: feed concentrations and temperature
- z=L: axial derivatives of concentrations and temperature are zero (the Danckwerts' closed boundary condition)
- r=0: symmetry condition given by radial derivatives of concentrations and temperature as zero
- r=R: concentration and temperature derivatives are zero and heat flux takes place to the jacket
- r_p=0: symmetry given by zero-derivatives of both concentration and temperatures
- r_p=R_p: continuity equations being the contact between the gas and the solid. No eventual film resistance was considered.

Several physical properties are needed for the computations. The pressure drop was calculated using the Ergun equation,

$$\Delta p / L = f_p \frac{\rho_G {u_G}^2}{d_p} \left(\frac{1-\varepsilon_G}{{\varepsilon_G}^3} \right) \tag{41}$$

where the friction factor (f_p) is given by Eq. 42.

$$f_p = \frac{150}{\mathrm{Re}_p} + 1.75, \mathrm{Re}_p = \frac{\rho u_G d_p}{(1-\varepsilon_G)\mu_G} \tag{42}$$

By applying Eq. 41, the generated pressure drop over the packed bed became 0.03 bar, due to the low density and viscosity of the gas.

The effective thermal conductivity of the packed bed was calculated weighting the gas and the solid conductivities, according to Eq. 43.

$$\lambda_B = \lambda_G (\lambda_S / \lambda_G)^{(1-\varepsilon_S)} \quad (43)$$

Molecular diffusivities were calculated from the Fuller-Schettler-Giddings equation[57]

$$D_{A,B} = \frac{0.00143T^{1.75}}{M_{AB}^{1/2}(\sum v_A^{1/3} + \sum v_B^{1/3})^2}, M_{AB} = 2\left(\frac{1}{M_A} + \frac{1}{M_B}\right)^{-1} \quad (44)$$

The atomic diffusion volume increments were: carbon: 16.5, oxygen: 5.48, hydrogen: 1.98, and helium: 2.88. The other physical properties needed are reported in Table 8, at 125 or 250°C.

Table 8 – Physical properties at 125 or 250°C and 1 bar of pressure. Gas density calculated by the ideal gas law (low value because helium was used as a reaction medium).

Parameter	Value	Unit
ρ_G	0.35, 0.27	kg/m^3
μ_G	$1.3\cdot10^{-5}$, $1.8\cdot10^{-5}$	kg/(m·s)
$c_{p,G}$	34, 34.5	J/(mol·K)
$c_{p,B}$	2000	J/(kg·K)
D_{EtOH}, $D_{Aldehyde}$, $D_{EtAcetate}$	1, 1.6	cm^2/s
D_{H2O}, D_{O2}	1.9, 3 – 1.6, 3	cm^2/s
$\Delta H_{r,1}$	$-51.0\cdot10^3$	J/mol
$\Delta H_{r,2}$	$-267.0\cdot10^3$	J/mol
$\Delta H_{r,3}$	$-34.3\cdot10^3$	J/mol

Other important parameters are listed in Table 9, including the reactor and particle dimensions, operation conditions and heat transfer parameters.

[57] R.C. Reid, J.M. Prausnitz, B.E. Poling. The Properties of Gases & Liquids (4th edition). McGraw-Hill, New York: **1958**.

Table 9 – Reactor/catalyst properties, heat and mass transfer parameters, initial and operation conditions.

Mass and heat transfer			**Reactor and catalyst**			**Initial conditions for each phase**		
Pe_G	10	-	L	$8 \cdot 10^{-3}$	m	u_G^0	0.03	m/s
λ_B	0.15	W/(m·K)	R	$5 \cdot 10^{-3}$	m	$C_{EtOH,G}^0$	2.3	mol/m³
			R_P	$3.15 \cdot 10^{-5}$	m	$C_{H2O,G}^0$	0	mol/m³
			w_{cat}	$0.16 \cdot 10^{-3}$	kg	$C_{Aldehyde,G}^0$	0	mol/m³
			ε_G	0.6	-	$C_{Acid,G}^0$	0	mol/m³
			ε_S	0.4	-	$C_{EtAcetate,G}^0$	0	mol/m³
			s	2	-	$C_{O2,G}^0$	2.3 or 7	mol/m³
						p	1	atm
						T_B^{IN}	125-250	°C

4.3 Ethanol partial oxidation kinetics

Tesser et al. [58] have published interesting results dealing with the partial oxidation of ethanol catalyzed by vanadium on titania. The authors reported an overall reaction network, where possible decomposition reactions to CO_2 are considered.

- $CH_3CH_2OH + 0.5\ O_2 \rightarrow CH_3CHO + H_2O$
- $CH_3CHO + 0.5\ O_2 \rightarrow CH_3COOH$
- $CH_3COOH + 2\ O_2 \rightarrow 2\ CO_2 + 2\ H_2O$
- $2\ CH_3CH_2OH + CH_3CHO \rightleftarrows CH_3CH(OCH_2CH_3)_2 + H_2O$
- $2\ CH_3CH_2OH \rightarrow CH_3CH_2OCH_2CH_3 + H_2O$

In the conditions adopted in the present work, we verified that no decomposition and no ether formation took place. Moreover, the gold catalyst favored the formation of acetaldehyde and acetic acid with traces of ethyl acetate. Thus, a simplified the reaction network was used as reported below:

1) Ethanol partial oxidation to acetaldehyde:

$$CH_3CH_2OH + 0.5\ O_2 \rightarrow CH_3CHO + H_2O$$

2) Acetaldehyde oxidation to acetic acid:

$$CH_3CHO + 0.5\ O_2 \rightarrow CH_3COOH$$

3) Ethyl acetate formation:

$$2\ CH_3CHO \rightarrow CH_3COOCH_2CH_3$$
$$CH_3CH_2OH + CH_3COOH \rightarrow CH_3COOCH_2CH_3 + H_2O$$

Concerning the ethyl acetate formation, two reactions can be taken into account: (i) the Tishchenko reaction in which an ester is formed by the disproportionation of two aldehyde molecules; (ii) the esterification of acetic acid with ethanol. Anyway, in the adopted reaction conditions only ethyl acetate traces were detected. Thus, discriminating among the two possible paths is practically impossible. Both of them have been

[58] R. Tesser, V. Maradei, M. Di Serio, E. Santacesaria. Kinetics of The Oxidative Dehydrogenation of Ethanol to Acetaldehyde on V_2O_5/TiO_2-SiO_2 Catalysts Prepared by Grafting. *Ind. Eng. Chem. Res.* **2004**, *43*, 1623-1633.

tested but in the present work only the results obtained by fixing the Tishchenko reaction will be shown.

Three different sets of rate equations were tested and compared using the developed PBR model. In particular, Mars-van Krevelen was chosen in agreement with Tesser et al. who proposed that the chemisorption of oxygen to from a vanadium peroxy radical, withdrawing the ethanol proton is the first step of the reaction, favoring the formation of acetaldehyde[58]. Langmuir-Hinshelwood-Hougen-Watson (LHHW) mechanism proposed by Sauer and Ollis was tested[59]. Finally, a power-law expression was chosen for comparison. The derived rate expressions are reported in Table 10.

Table 10 – Kinetic equations for the partial oxidation of ethanol (1), acetaldehyde oxidation (2), ethyl acetate formation (3).

Mars-van Krevelen	**Langmuir-Hinshelwood-Hougen-Watson**	**Power law**
$r_1 = \frac{k_1 p_{EtOH}}{1+\frac{k_1 p_{EtOH}}{k_2 p_{O_2}^{1/2}}}$	$r_1 = \frac{k_1' p_{EtOH} p_{O_2}^{1/2}}{(1+K_{EtOH} p_{EtOH} + (K_{O_2} p_{O_2})^{1/2} + K_{H_2O} p_{H_2O} + K_{Alde} p_{Alde})^2}$	$r_1 = k_1'' p_{EtOH} p_{O_2}^m$
$r_2 = \frac{k_3 p_{Alde}}{1+\frac{k_3 p_{Alde}}{k_2 p_{O_2}^{1/2}}}$	$r_2 = \frac{k_2' p_{Alde} p_{O_2}^{1/2}}{(1+K_{EtOH} p_{EtOH} + (K_{O_2} p_{O_2})^{1/2} + K_{H_2O} p_{H_2O} + K_{Alde} p_{Alde})^2}$	$r_2 = k_2'' p_{Alde} p_{O_2}^n$
$r_3 = k_3 p_{Alde}$	$r_3 = \frac{k_3' p_{Alde}}{(1+K_{EtOH} p_{EtOH} + (K_{O_2} p_{O_2})^{1/2} + K_{H_2O} p_{H_2O} + K_{Alde} p_{Alde})^2}$	$r_3 = k_3'' p_{Alde}$

Depending on the rate expressions, the reactant and product adsorption effects were considered or not.

[59] M.L. Sauer, D.F. Ollis. Photocatalyzed Oxidation of Ethanol and Acetaldehyde in Humidified Air. *Journal of Catalysis* **1996**, *158*, 570-582.

4.4 Screening of rate expressions

The rate expressions reported in the previous section were evaluated by conducting parameter estimations for available experimental data. The experimental data consisted of two series of steady-state data for conversion and yields, at a fixed oxygen-to-ethanol ratio (1 or 3), obtained by adjusting the reactor temperature step-wisely and gradually from 125°C to 250°C, passing from one set temperature value to another one. It was verified that the system attained the steady-state conditions at each temperature. The experiments were performed by using gold nanoparticles on HY-80 support served as the selected catalyst. Information about the catalyst and its characterization, being a part of another PhD thesis by E. Behravesh, is provided in **Publication IV**.

The experimental data useful for the parameter estimation are displayed in Figure 10.

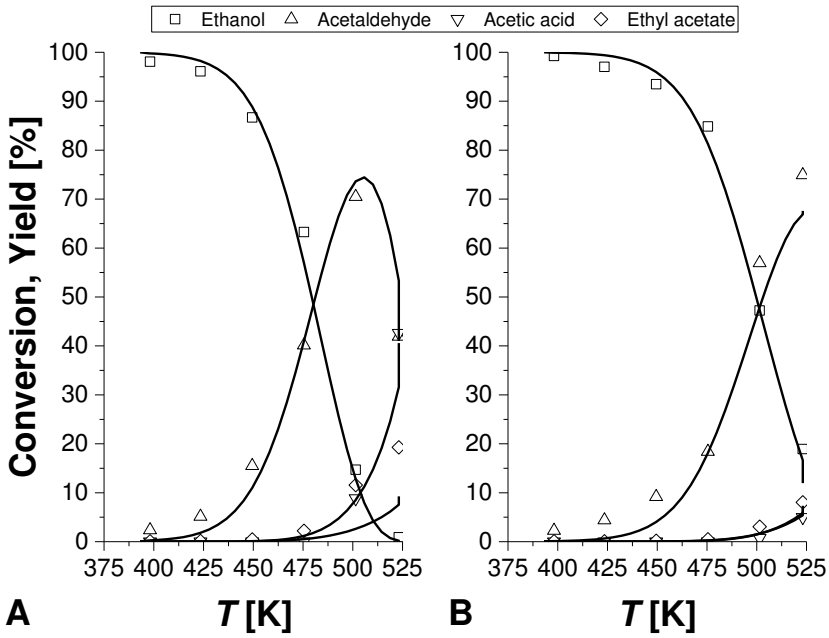

Figure 10 – Experimental data collected by fixing the oxygen-to-ethanol ratio of 3 (A) and 1 (B). The calculated profiles refer to the prediction of Langmuir-Hinshelwood-Hougen-Watson (LHHW) model.

A summary of the parameter estimation results is provided by Table 11.

Table 11 – Parameter estimation results based on the packed bed experimental data. Comparison of different kinetic equations. Reference temperature=403K.

Power Law		**Mars-van Krevelen**		**LHHW**	
$E_{a,1}$ [kJ/mol]	105	$E_{a,1}$ [kJ/mol]	123	$E_{a,1}$ [kJ/mol]	125.3
$E_{a,2}$ [kJ/mol]	108	$E_{a,2}$ [kJ/mol]	87	$E_{a,2}$ [kJ/mol]	112.3
$E_{a,3}$ [kJ/mol]	87	$E_{a,3}$ [kJ/mol]	71	$E_{a,3}$ [kJ/mol]	81.45
$k''_{1,ref}$ [mol/g/s/Pa^{m+1}]	$7.11 \cdot 10^{-5}$	$E_{a,O2ads}$ [kJ/mol]	34	$k'_{1,ref}$ [mol/g/s/Pa$^{1.5}$]	$3.36 \cdot 10^{-5}$
$k''_{2,ref}$ [mol/g/s/Pa^{n+1}]	$1.00 \cdot 10^{-6}$	$k_{1,ref}$ [mol/g/s/Pa]	$4.79 \cdot 10^{-6}$	$k'_{2,ref}$ [mol/g/s/Pa$^{1.5}$]	$6.13 \cdot 10^{-6}$
$k''_{3,ref}$ [mol/g/s/Pa]	$5.55 \cdot 10^{-5}$	$k_{2,ref}$ [mol/g/s/Pa$^{0.5}$]	$1.27 \cdot 10^{-5}$	$k'_{3,ref}$ [mol/g/s/Pa]	$2.40 \cdot 10^{-4}$
m [-]	1.81	$k_{3,ref}$ [mol/g/s/Pa]	$3.10 \cdot 10^{-6}$	K_{EtOH} [1/Pa]	$1.53 \cdot 10^{-2}$
n [-]	0.78	$k'_{4,ref}$ [mol/g/s/Pa]	$1.98 \cdot 10^{-6}$	K_{O2} [1/Pa]	$1.00 \cdot 10^{-4}$
				K_W [1/Pa]	$2.00 \cdot 10^{-3}$

The activation energies can be compared as follows. In particular, the activation energies for the partial oxidation of ethanol and oxidation of aldehyde were around 105-125 kJ/mol and 100 kJ/mol respectively, while the condensation of aldehydes is less probable than the esterification. The estimated oxygen reaction order (m) is not very reliable, being the molecularity 0.5. This is certainly due to the high correlation of the parameters for the power law approach.

The agreement between the experimental data and the model is very similar for the different models. As an example, the profiles obtained with the LHHW rate laws are reported in Figure 10. Similar curves are presented in **Publication IV**.

The three approaches were able to follow closely the experimental observations. Ethanol conversion increases as the set temperature was increased. Acetaldehyde is the first product observed when increasing temperature. At temperatures exceeding 200°C, the acetic acid generation became consistent. Finally, in case of the oxygen excess, the oxidation reactions started to progress at lower temperatures.

The main reason why the results are similar is that the experiments were performed by using 80% dilution with the inert gas. Thus, the system is rather diluted and eventual adsorption effects are suppressed.

4.5 Parametric study

A parametric study was performed to highlight two main issues: the influence of the catalyst loading and the effect of the uncertainty in the Péclet number. For this purpose, two simulations were carried out by varying the catalyst loading. The results are displayed in Figure 11.

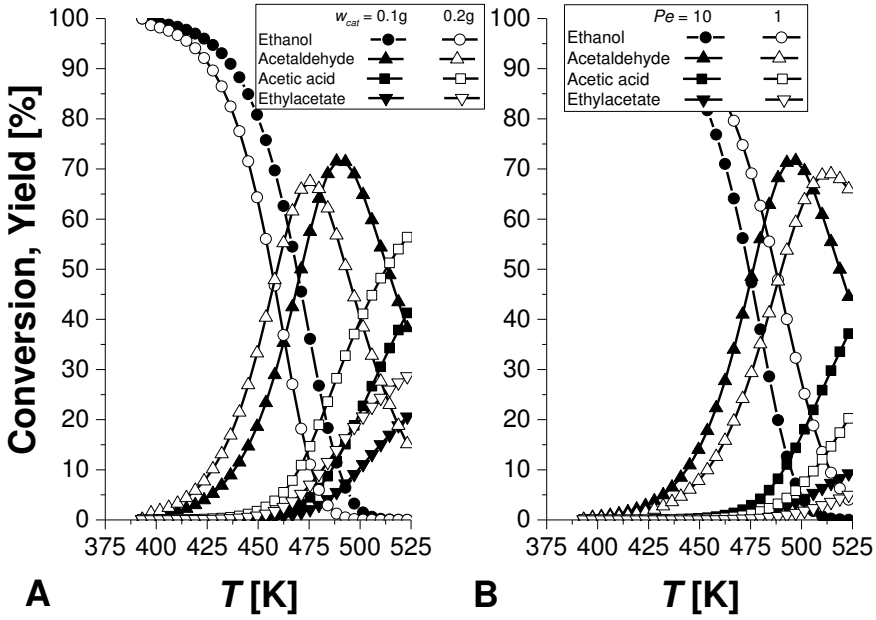

Figure 11 – Parametric study. A. Influence of the catalyst loading. B. Influence of the Péclet number.

It was observed (Figure 11A) that the reaction rates increased as the catalyst loading was doubled. The acetaldehyde maximum is shifted towards lower temperatures.

Finally, as the Péclet number was decreased from 10 to 1, the productivity was suppressed and higher temperatures were needed to reach similar yields (Figure 11B). The discussion clearly indicates that an a-priori determination of this parameter is crucial for a correct interpretation of the experimental data.

4.6 Conclusions

A general packed bed reactor model was developed and tested with experimental data. The model was based on the dynamic solution of mass and heat balance equations, including both axial and radial dispersion terms. The model is general and it can be applied to describe any experiments performed in catalytic fluid-solid systems.

As a demonstration, it was applied to the partial oxidation of ethanol on gold nanoparticles as a case study. Different rate expressions were screened. In all the cases the agreement between the model prediction and the experimental data was very satisfactory. A final parametric investigation demonstrated the effect of the key parameters on the simulated results.

List of symbols

A_P	Particle surface area, [m^2]
cat	Catalyst
$C_{i,G}$	Concentration of component *i* in gas, [mol/m^3]
$C_{i,S}$	Concentration inside catalyst particles,[mol/m^3]
$C_{p,G}$	Specific heat of phase, [$J/(kg \cdot K)$]
$C_{p,B}$	Specific heat of reactor bed, [$J/(kg \cdot K)$]
$D_{eff,i}$	Effective diffusivity of component *i*, [m^2/s]
D_i	Molecular diffusivity of component *i* in gas-phase, [m^2/s]
$D_{A,B}$	Molecular diffusivity of component A in B, [m^2/s]
d_p	Particle diameter, [m]
$D_{r,G}$	Radial dispersion coefficient, [m^2/s]
$D_{z,G}$	Axial dispersion coefficient, [m^2/s]
$E_{a,j}$	Activation energy of reaction *j*, [J/mol]
f_p	Friction factor, [-]
i	Component
k_1	Mars-van Krevelen rate parameter, [$mol/(g_{cat} \cdot s \cdot bar)$]
k_2	Mars-van Krevelen rate parameter, [$mol/(g_{cat} \cdot s \cdot bar^{0.5})$]
k_3	Mars-van Krevelen rate parameter, [$mol/(g_{cat} \cdot s \cdot bar)$]
k'_1	LHHW rate parameter, [$mol/(g_{cat} \cdot s \cdot bar^{1.5})$]
k'_2	LHHW rate parameter, [$mol/(g_{cat} \cdot s \cdot bar^{1.5})$]
k'_2	LHHW rate parameter, [$mol/(g_{cat} \cdot s \cdot bar)$]
k''_1	Power law rate parameter, [$mol/(g_{cat} \cdot s \cdot bar^{m+1})$]
k''_2	Power law rate parameter, [$mol/(g_{cat} \cdot s \cdot bar^{n+1})$]
k''_3	Power law rate parameter, [$mol/(g_{cat} \cdot s \cdot bar)$]
$k_{j,ref}$	Mars-van Krevelen rate parameter at reference temperature
$k'_{j,ref}$	LHHW rate parameter at reference temperature
$k''_{j,ref}$	Power law rate parameter at reference temperature
K_i	Adsorption parameter for component *i*, [1/bar]
L	Reactor length, [m]
m	Power law exponent, [-]
M_A, M_B	Molecular mass of component A and B, [g/mol]
M_{AB}	Mean molecular mass, [g/mol]
n	Power law exponent, [-]
$N_{G,S,i}$	Solid to gas molar flux of component *i*, [$mol/(m^3 \cdot s)$]
p	Pressure, [bar]

p_i	Partial pressure of component *i*, [bar]
Pe_G	Péclet number for gas, [-]
r	Radial location, [m]
R	Reactor radius, [m]
Re_p	Modified particle Reynolds number, [-]
r_j	Reaction *j* rate, [mol/(g·s)]
r_p	Radial location within particle, [m]
R_P	Particle radius, [m]
s	Shape factor, [-]
t	Time, [s]
T_B	Bed temperature, [°C]
T_B^{IN}	Initial bed temperature, [°C]
u_G^0	Feed velocity of the gas phase, [m/s]
u_G	Superficial gas velocity, [m/s]
V_P	Particle volume, [m^3]
w_{cat}	Catalyst mass, [kg]
z	Axial location, [m]

Greek symbols

$\Delta H_{r,j}$	Reaction enthalpy of reaction *j*, [kJ/mol]
Δp	Pressure drop, [Pa]
ε_G	Holdup of gas-phase, [-]
ε_S	Holdup of solid-phase, [-]
μ_G	Viscosity of gas-phase, [Pa·s]
$\lambda_G, \lambda_S, \lambda_B$	Thermal conductivity of gas, solid, bed, [W/(m·K)]
$\lambda_{r,B}$,$\lambda_{z,B}$	Radial and axial thermal conductivity of the bed, [W/(m·K)]
ρ_{cat}	Catalyst concentration, [kg/m^3]
ρ_G, ρ_S, ρ_B	Density of gas, solid and bed, [kg/m^3]
$\nu_{i,j}$	Stoichiometric coefficient component *i* reaction *j*, [-]
$\sum \nu_i$	Sum of atomic contribution factors, *i* = A or B

Chapter 5 – Shrinking particle model: limestone dissolution in acidic environment

"Science is no more than an investigation of a miracle we can never explain, and art is an interpretation of that miracle."

Ray Bradbury, The Martian Chronicles, 1950

5.1 Introduction

The topic of the present chapter is the development and use of an extended shrinking film model (E.S.F.M.). The fundamental idea was to start from the well-known theory of gas-liquid films[60,61,62,63], but extend it to the case where the solid component acts as a reactant, which firstly dissolves and then reacts with the components present in the liquid phase. If the reaction is rapid, it can occur both in the liquid bulk and in the stagnant film surrounding the solid particle. As the reaction proceeds, the particles diminish in size and the film surrounding the particle becomes thinner and thinner.

As the reaction progresses the reactant concentration diminishes and the reaction rates decline. Coupling of this effect to the decrease of the film thickness shifts the overall reaction network from the liquid film to the bulk phase. Moreover, depending on the stirring rate, it is possible to pass from a film to a bulk dominating process. Thus, if the liquid-phase turbulence is sufficiently high (typical for laboratory-scale reactors), the film around the particle diminishes in size and the chemical processes move to the bulk phase; on the contrary, for less stirred systems (industrial-scale), the film reaction can dominate the overall rate.

It is evident that such models can be useful for the scale-up fluid-solid reactions, in which the solid phase acts as a reactant. In the present part of the work, a shrinking particle model was developed, testing it first by generic simulations, highlighting the influence of the main operation conditions. In the next stage, the model was applied in describing a case study of interest, that is the limestone dissolution in acidic environment.

---

[60] R. Higbie. The Rate of Absorption of a Pure Gas into Still Liquid During Short Periods of Exposure. *Trans. Am. Inst. Chem. Eng.* **1935**, *35*, 365.
[61] P.V. Danckwerts. Gas-Liquid Reactions. McGraw Hill, New York: **1970**.
[62] O. Levenspiel. Chemical Reaction Engineering (3rd edition). John Wiley & Sons Inc., New York: **1990**.
[63] P. Trambouze, H. van Landeghem, J.P. Wauquier. Chemical Reactors: Design, Engineering, Operation. Editors Technip, Paris: **1988**.

5.2 Shrinking particle model

The shrinking particle model is based on some main assumptions, which are listed below:

- The reaction is rapid occurring both in the film and the bulk phases
- The system is isothermal
- The particles have equal sizes
- The liquid bulk phase is well-stirred

For the sake of illustration, a schematic picture of a generic particle, for which the calculation coordinates are explained, is displayed in Figure 12.

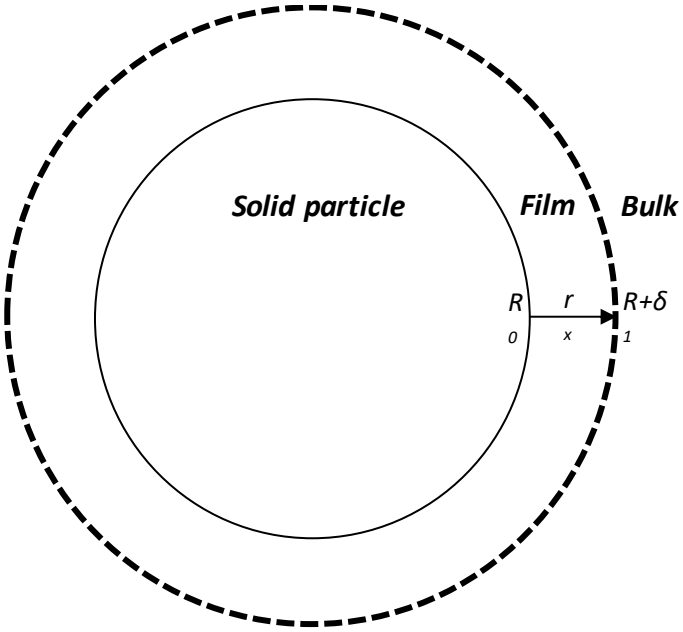

Figure 12 – A principal sketch of the shrinking particle-shrinking film model.

5.2.1 Mass balance equations

As the system is composed by three phases (solid particle, liquid film and liquid bulk), three different mass balances are considered.

The mass balance for a dissolved component (i) can be written as in Eq. 45.

$$\frac{\partial c_i}{\partial t} = D_i\left(\frac{\partial^2 c_i}{\partial r^2} + \frac{s}{r}\frac{\partial c_i}{\partial r}\right) + r_j, \quad R \le r \le R + \delta \tag{45}$$

For instance, the accumulation term is given by the net sum of two contributions, i.e. the film reaction rate and the diffusion inside the film itself, given by Fick's law. The shape factor is s=2 for a spherical particle, s=1 for a long cylinder, s=0 for a slab. The shape factor can be even larger than 2, or even non-integer, for a real particle with surface defects[64].

As stated previously, when the reaction proceeds, the particle becomes smaller and the film thickness diminishes. Thus the upper coordinate of the PDE varies with time. Solving such a system can become numerically challenging. For this reason, a dimensionless film coordinate (x) is introduced, defined as $x=(r-R)/\delta$, where δ is the film thickness. After some mathematical rearrangements, Eq. 45 becomes

$$\frac{\partial c_i}{\partial t} = \frac{D_i}{\delta^2}\left(\frac{\partial^2 c_i}{\partial x^2} + \frac{s\delta}{R + \delta x}\frac{\partial c_i}{\partial x}\right) + r_j, \ 0 \le x \le 1 \tag{46}$$

The following boundary conditions are needed to solve the PDE.

- x=0: $c_i = c^*_i$ (saturation of the solid components at the surface)
- x=0: $\partial c_i/\partial x = 0$ (liquid-phase component at the surface)
- x=1: $c_i = c'_i$ (bulk-phase conditions valid at the end of the film)

[64] T. Salmi, H. Grénman, H. Bernas, J. Wärnå, D. Murzin. Mechanistic Modelling of Kinetics and Mass Transfer for A Solid–Liquid System: Leaching of Zinc with Ferric Iron. *Chem. Eng. Sci.* **2010**, *65*, 4460-4471.

Eq. 46 can be re-written in a dimensionless form, by dividing the concentrations by their initial values, and the reaction time by a characteristic time (τ), obtaining Eq. 47.

$$\frac{\partial y_i}{\partial \theta} = \frac{D_i \tau}{R_0{}^2 (\delta / R_0)^2} \left(\frac{\partial^2 y_i}{\partial x^2} + \frac{s(\delta / R_0)}{R / R_0 + (\delta / R_0) x} \frac{\partial y_i}{\partial x} \right) + r_j \frac{\tau}{c_0} \qquad (47)$$

As revealed by Eq. 47, $D_i \tau / R_0^2$ is the first dimensionless number defined in this context.

The film thickness, δ, is calculated by using the standard correlation relating the Sherwood number (*Sh*) to the Reynolds (*Re*) and Schmidt (*Sc*) numbers[65],

$$Sh = a' + b' \mathrm{Re}^{\alpha'} Sc^{\beta'} \rightarrow \frac{k_{Li} d}{D_i} = 2 + \left(\frac{\varepsilon d^4}{\upsilon^3} \right)^{1/6} \frac{\upsilon}{D_i}^{1/3} \qquad (48)$$

According the to the film theory, the film thickness is defined as $\delta = D_i / k_{Li}$. The expression for the Reynolds number is based on the turbulence theory of Kolmogoroff valid for agitated slurry reactors[66]. The exponents $\alpha' = 1/6$ and $\beta' = 1/3$ were proposed by Temkin for liquid-phase systems[66]. Under silent conditions, $Sh \rightarrow 2$, thus $a' = 2$, while $b' = 1$ is used for the sake of simplicity.

By rearranging Eq. 48, the film thickness can be obtained as in Eq. 49.

$$\delta = 2R \left[2 + \left(\frac{\varepsilon}{\upsilon^3} \right)^{1/6} \left(\frac{\upsilon}{D_i} \right)^{1/3} (2R)^{2/3} \right]^{-1} \qquad (49)$$

Hence, the film thickness depends on physical properties, such as the particle radius (*R*), the kinematic viscosity of the fluid (υ), the molecular diffusivity (D_i), and on the energy dissipated (ε).

---

[65] N. Wakao. Recent Analysis of Chemically Reacting Systems. Wiley Eastern, New Delhi: **1984**.
[66] M.I. Temkin. Transfer of Dissolved Matter Between a Turbulently Moving Liquid and Particles Suspended in It. *Kinetika i Kataliz* **1977**, *18*, 493-496.

Concerning the dissipated energy, two extreme cases are of interest, for both silent (ε=0) and vigorously agitated (ε>>100) cases, as given by Eq. 50.

$$\delta = \begin{cases} \varepsilon = 0,\ \delta = R \\ \varepsilon >> 100,\ \delta = (2R)^{1/3}\left(\left(\frac{\varepsilon}{\upsilon^3}\right)^{1/6}\left(\frac{\upsilon}{D_i}\right)^{1/3}\right)^{-1} \end{cases} \tag{50}$$

For calculation purposes, it is strongly suggested to express the particle radius as a function of the amount of solid substance, which can be calculated by using Eq. 51, valid for both a generic time and t=0,

$$n_j(t) = \frac{n_P \rho_P V_P(t)}{M_P} \tag{51}$$

For a particle of arbitrary geometry $V_P/V_{0P}=(R/R_0)^{s+1}$, therefore the ratio n_j/n_{0j} becomes

$$\frac{n_j}{n_{0j}} = \left(\frac{R}{R_0}\right)^{s+1} \tag{52}$$

This relation is introduced in Eq. 49, giving the final film thickness expression, Eq. 53.

$$\delta = R_0\left(\frac{n_j}{n_{0j}}\right)^{1/(s+1)}\left[1+\left(\frac{\varepsilon}{\upsilon^3}\right)^{1/6}\left(\frac{\upsilon}{D_i}\right)^{1/3}\left(\frac{{R_0}^2}{2}\right)^{1/3}\left(\frac{n_j}{n_{0j}}\right)^{2/(3(s+1))}\right]^{-1} \tag{53}$$

A dimensionless form can be obtained as shown in Eq. 54.

$$\frac{\delta}{R_0} = \frac{\left(\frac{n_j}{n_{0j}}\right)^{1/(s+1)}}{1+\left(\frac{\varepsilon}{\upsilon^3}\right)^{1/6}\left(\frac{\upsilon}{D_i}\right)^{1/3}\left(\frac{{R_0}^2}{2}\right)^{1/3}\left(\frac{n_j}{n_{0j}}\right)^{2/(3(s+1))}} = \frac{\left(\frac{n_j}{n_{0j}}\right)^{1/(s+1)}}{1+\alpha\left(\frac{n_j}{n_{0j}}\right)^{2/(3(s+1))}} \tag{54}$$

where α is the second dimensionless number.

The liquid bulk phase mass balance can be written as

$$\frac{dc'_i}{dt} = r'_j + N'_i a_P \tag{55}$$

The overall mass balance originates from the idea that the accumulation term is given by the net sum of the reaction rate and the flux from the film phase. Recalling that $a_P=A_P/V_L$ the total particle surface area-to-liquid volume ratio, and by considering that for a spherical particle $A_P(t)=n_P 4\pi R(t)^2$, $a_P/a_{0P}=(R/R_0)^2$. For a general geometry $a_P/a_{0P}=(R/R_0)^s$. Thus, after rearranging Eq. 55, inserting also Eq. 52, Eq. 56 is obtained.

$$\frac{dc'_i}{dt} = r'_j + N'_i a_0 \left(\frac{n_j}{n_{0j}}\right)^{s/(s+1)}, \quad N'_i = -\frac{D_i}{\delta}\frac{\partial c_i}{\partial x}\bigg|_{x=1} \tag{56}$$

The corresponding dimensionless form is shown in Eq. 57.

$$\frac{dy'_i}{d\theta} = r'_j \frac{\tau}{c_0} - \left(\frac{D_i a_0 \tau / R_0}{\delta / R_0}\right)\left(\frac{n_j}{n_{0j}}\right)^{s/(s+1)} \frac{\partial y_i}{\partial x}\bigg|_{x=1} \tag{57}$$

Where $D_i a_0 \tau/R_0$ is the third dimensionless number.

Finally, the solid phase mass balance can be written as in Eq. 58.

$$\frac{dn'_j}{dt} + N_j A = 0, \quad N_j = -\frac{D_j}{\delta}\frac{\partial c_j}{\partial x}\bigg|_{x=0} \tag{58}$$

No reaction is presumed to take place inside the solid phase; thus, the accumulation term is given by the material flux to the film phase at the outer surface of the particle. The outer surface area is given by $A=a V_L=a_0(R/R_0)^s V_L$. After inserting Eq. 52 to Eq. 58, the final form of the mass balance can be obtained (Eq. 59).

$$\frac{dn'_j}{dt} = \left(\frac{D_j a_0 V_L}{\delta}\right)\left(\frac{n_j}{n_{0j}}\right)^{s/(s+1)} \left.\frac{\partial c_j}{\partial x}\right|_{x=0} \tag{59}$$

The related dimensionless form becomes,

$$\frac{dn'_j / n_{0j}}{d\theta} = \left(\frac{D_j a_0 \tau / R_0}{\delta / R_0}\right)\left(\frac{c_0 V_L}{n_{0j}}\right)\left(\frac{n_j}{n_{0j}}\right)^{s/(s+1)} \left.\frac{\partial y_j}{\partial x}\right|_{x=0} \tag{60}$$

where $c_0 V_L / n_{0j}$ is the fourth dimensionless number.

Further details on the derivation of the mass balance equations can be found in **Publication V**.

The presented set of ordinary differential equations (ODEs) and parabolic partial differential equations (PDEs) were solved numerically by using the advanced modelling tool gPROMS Model Builder v.4.0 software[32]. The PDEs system was solved with the built in numerical method of lines, using the second order centered finite difference formulae for the spatial derivatives, with 40 discretization points along the dimensionless coordinate (x) of the film.

5.2.2 Contribution analysis

In the developed E.S.F.M., the reaction proceeds simultaneously in both the stagnant film surrounding the solid particle and the liquid bulk phase. Thus, it is interesting to discriminate the extent of the reaction in each phase in a practical way. For this reason, contribution analysis was introduced, starting from the momentaneous contributions (κ) of the reaction in each phase, according Eqs. 61-62.

$$\kappa_{kF} = \int_0^{V_F} r_k dV_F = 4\pi \int_0^1 r_k (x\delta + R)^2 \delta dx \tag{61}$$

$$\kappa_{kB} = r'_k V_L \tag{62}$$

The infinitesimal volume element of the film can be obtained from geometrical considerations. Thus, Eq. 61 can be rewritten by expressing the momentaneous contribution of the film by the dimensionless coordinate (x) for a spherical particle.

The relative contributions of respectively the film and bulk reactions can be calculated from their relative ratios, as explained by Eqs. 63-64.

$$\lambda_{kF} = \frac{\int_0^{V_F} r_k dV_F}{\int_0^{V_F} r_k dV_F + r'_k V_L} \tag{63}$$

$$\lambda_{kB} = \frac{r'_k V_L}{\int_0^{V_F} r_k dV_F + r'_k V_L} \tag{64}$$

These dimensionless quantities range from 0 to 1, with the boundaries indicating the complete dominance of either the film or the bulk phase.

Further details on the contribution analysis can be found in **Publication V**.

5.3 Parametric study for a bimolecular reaction

A parametric study was conducted to illustrate the performance of the new shrinking particle model. The effect of several parameters was checked with a dedicated investigation program, by assuming that a bimolecular reaction proceeds both in the stagnant film and in the bulk phase. The reaction scheme is displayed below.

1. $B_S \rightarrow B$		Dissolution
2. $A + B \rightarrow C$	(Film)	$r_1 = k \cdot c_A(x) \cdot c_B(x)$
3. $A + B \rightarrow C$	(Bulk)	$r_1' = k \cdot c'_A \cdot c'_B$

A synopsis of the parameter values used in the simulations is reported in Table 12.

Table 12 – Parameters used to perform the parametric study. V_L=1·10^{-5}m^3, c^*=1·10^{3}mol/m^3, c_0=1·10^{3}mol/m^3, s=3, $AD4=c_0V_L/n_0$=1, $AD3=\alpha$=0 (stagnant case). $AD1=D_i\tau/R_0^2$, $AD2=D_ia_0\tau/R_0$.

SIM	k [m^3/mol/s]	D_i [m^2/s]	R_0 [m]	*AD1* [-]	*AD2* [-]
1	1·10^{-2}	1·10^{-9}	1·10^{-4}	1·10^{-1}	2·10^{-2}
2	1·10^{-2}	1·10^{-8}	1·10^{-4}	1·10^{0}	2·10^{-1}
3	1·10^{-2}	1·10^{-9}	1·10^{-3}	1·10^{-3}	2·10^{-4}
4	1·10^{-2}	1·10^{-8}	1·10^{-3}	1·10^{-2}	2·10^{-3}
5	1·10^{-1}	1·10^{-9}	1·10^{-4}	1·10^{-1}	2·10^{-3}
6	1·10^{-1}	1·10^{-8}	1·10^{-4}	1·10^{0}	2·10^{-1}
7	1·10^{-1}	1·10^{-9}	1·10^{-3}	1·10^{-3}	2·10^{-4}
8	1·10^{-1}	1·10^{-8}	1·10^{-3}	1·10^{-2}	2·10^{-3}
9	1·10^{-3}	1·10^{-9}	1·10^{-4}	1·10^{-1}	2·10^{-2}
10	1·10^{-3}	1·10^{-8}	1·10^{-4}	1·10^{0}	2·10^{-1}
11	1·10^{-3}	1·10^{-9}	1·10^{-3}	1·10^{-3}	2·10^{-4}
12	1·10^{-3}	1·10^{-8}	1·10^{-3}	1·10^{-2}	2·10^{-3}

A wide range of parameters was investigated. To calculate a_0, the molecular mass of the solid was considered to be 0.1 kg/mol, while the solid density was assumed to be 2000 kg/m^3 was assumed.

Examples of simulated dimensionless concentration profiles within the film phase for each component are displayed in Figure 13A-C, referred to simulation 1 output.

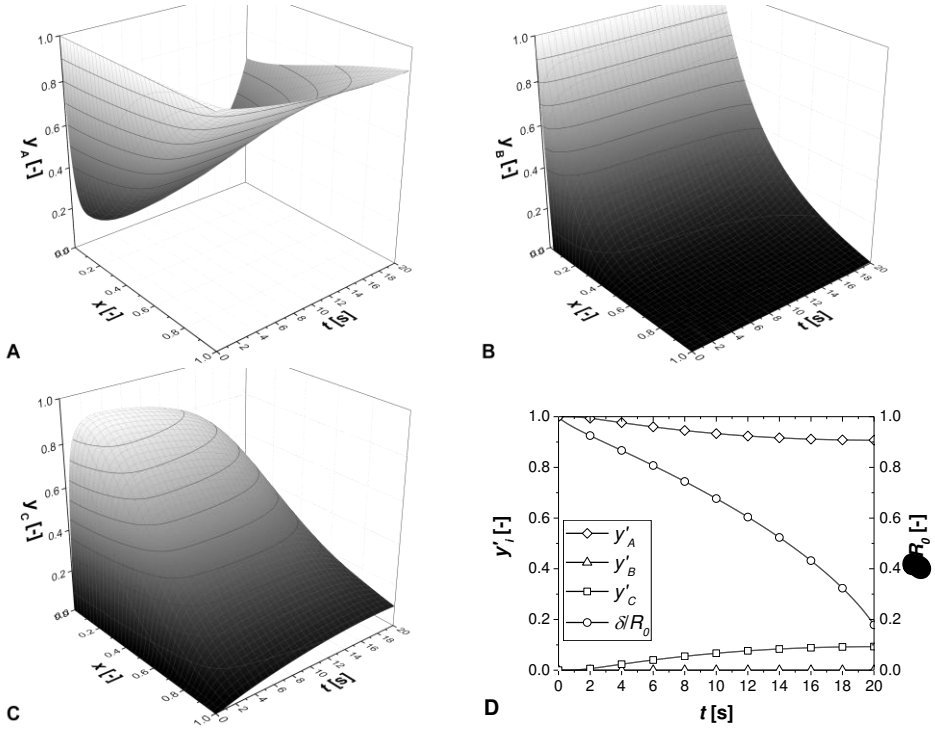

Figure 13 – A-C: Plot of the dimensionless concentration of the three components within the phase as a function of the reaction time and dimensionless film thickness. D: Dimensionless concentrations and dimensionless film thickness profiles.

The results are consistent from a qualitative view point. As a matter of fact, the concentration of the dissolved reactant (B) decreases with time exhibiting its maximum at x=0, i.e. at the outer surface of the solid. Components A and C present similar trends but opposite, being the reactant and the product, respectively. In Figure 13D, the dimensionless concentrations for each component in the bulk phase are displayed. It follows from the simulations for no mixing case, B is non-accumulated in the bulk phase. Moreover, as the reaction proceeds, the film thickness diminishes as expected (Figure 13D).

A very interesting result is revealed by Figure 14, where the *AD1* and *AD2* values (corresponding to D_i and R_0 variation) are reported against

the particle radius conversion calculated at t=1s. The curves are parametric respect to the kinetic constant.

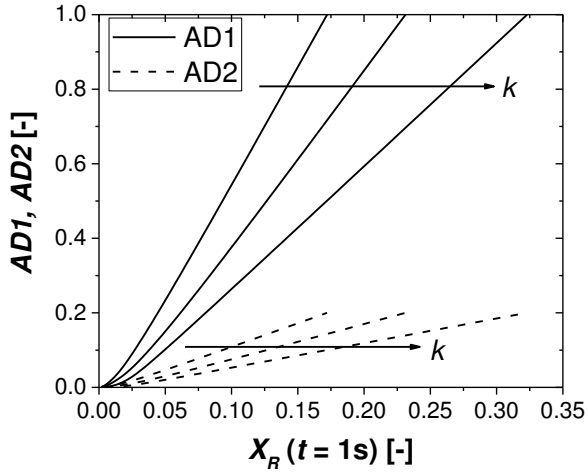

Figure 14 – Dimensionless numbers as a function of the particle radius conversion (X_R) evaluated at t=1s, by fixing different kinetic constant values.

The figure reveals that the dependencies are not linear. At a fixed value of the kinetic constant, the particle radius conversion increases with the dimensionless numbers, proportional to D_i and R_0. Moreover, by fixing the physical parameters (*AD1* and *AD2*), the particle conversion increases accordingly. The mentioned aspects show the high flexibility of the model in describing different chemical and physical systems.

The effect of the particle radius on the film concentration profiles along with the related contribution analysis is reported in Figure 15.

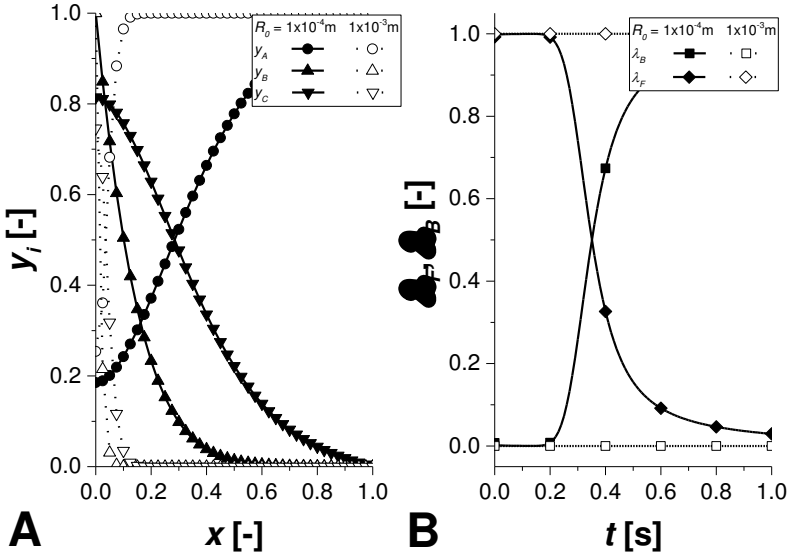

Figure 15 – A. Dimensionless concentration profiles at 1s in the liquid film for different R_0 values. B. Results from the contribution analysis. The conditions correspond to simulations 1 and 3.

The results reveal that by increasing the radius, R_0, the solid component dissolution becomes significantly slower, leading to a slower formation of the liquid-phase product. The result is expected because smaller particles have thinner films, and the diffusion path becomes shorter during the progress of the reaction. The contribution analysis confirms this aspect. Smaller particles show an inversion of the contribution, switching from a film to bulk-phase dominance at shorter reaction times.

Further simulation results, concerning the effect of the shape factor and the stirring rate, can be found in **Publication V**. It was decided to present in this chapter only some examples of the obtained results, to elucidate the treatise of the subject. The stirring rate effect will be also discussed in the next section for a real case study.

5.4 Limestone dissolution in acidic environment

Limestone dissolution in the presence of hydrochloric acid (HCl) is a particularly well-suited system as a case study to be described with the developed shrinking particle model. The system is of particular relevance because the limestone dissolution kinetics is still not very well understood even though this reaction is a key step in sulfur dioxide removal technology. Several simplified kinetic models have been employed, which do not take into account the physical phenomena involved[71].

The idea is to apply the developed model to reveal the intrinsic kinetics. The overall reaction mechanism consists of the following steps:

1. $CaCO_{3(S)} \rightleftarrows Ca^{2+}_{(L)} + CO_3^{2-}{}_{(L)}$:
2. $CO_3^{2-}{}_{(L)} + H^+ \rightleftarrows HCO_3^-$
3. $HCO_3^- + H^+ \rightleftarrows CO_2 + H_2O$
4. $HCO_3^- + H^+ \rightleftarrows H_2CO_3$

Step 1 is the limestone dissociation, which can be considered rapid in a well-stirred system. Step 2 is an acid catalyzed reaction, which can be considered as the rate determining step of the overall dissolution. Apparent first order kinetics with respect to the proton concentration was observed for the reaction rate[67,68,69] at a low pH, also in the present work[71]. Reaction 2 can be considered irreversible within the studied pH range, as the backward reaction is thermodynamically favored only at a high pH[70]. Further rapid proton equilibria can prevail, depending on the pH (steps 3-4)[70]. These rapid protonation reactions are assumed to be in quasi-equilibria and, thus, not influence directly the dissolution kinetics.

---

[67] P. Barton, T. Vatanatham. Kinetics of Limestone Neutralization of Acid Waters. *Environ. Sci. Technol.* **1976**, 10, 262-266

[68] J. Ahlbeck, T. Engman, S. Faltén, M. Vihma. Measuring the Reactivity of Limestone for Wet-flue Gas Desulfurization. *Chem. Eng. Sci.* **1995**, *50*, 1081–1089

[69] L.N. Plummer, T.M.L. Wigley, D.L. Parkhurst. The Kinetics of Calcite Dissolution in CO_2 Water Systems At 5 and 60°C And 0.0 To 1.0atm CO_2. *Am. J. Sci.* **1978,** *278*, 179-216.

[70] L.N. Plummer, E. Busenberg. The Solubilities Of Calcite, Aragonite and Vaterite In CO_2-H_2O Solutions Between 0 And 90°C, and an Evaluation of The Aqueous Model for The System $CaCO_3$-CO_2-H_2O. *Geochim. Cosmochim. Acta* **1982**, *46*, 1011-1040.

For the mentioned reasons, we adopted the rate expressions reported in Eq. 65.

$$r = kc_{H^+}c_S, r' = kc_{H^+}{}'c_S{}' \tag{65}$$

The experimental data to be interpreted were recently published by our group[71]. Two different natural limestone samples originating from Pargas (Parainen, Finland) and Wolica (Poland) were used, with two different granulometric sizes, namely "small" (74-125μm) and "large" (212-250μm). The experiments were conducted in a 2L jacketed batch reactor, where 1g of limestone sample was placed in contact with 1.5L of a pre-heated HCl solution. The pH of the solution was constantly monitored on-line till reaching a stable value (from pH≅2-3 to pH≅7), corresponding to almost complete HCl conversion and roughly 30-40% of solid conversion. Experimental data were collected in a wide range of operation conditions, i.e. varying temperature, particle size, stirring rate and limestone type. The main experimental conditions are summarized in Table 13.

The authors verified that only a minor improvement was observed varying the stirring rate from 1600 to 1800 rpm[71]. Thus, the majority of experiments were performed at 1600 rpm.

The diffusivities of the ionic species were estimated from the classical Nernst-Haskell correlation[24],

$$D^0_{AB} = \frac{RT[(1/z_+) + (1/z_-)]}{F^2[(1/\lambda^0_+) + (1/\lambda^0_-)]} = a_i T \tag{66}$$

This correlation predicts a linear dependence with temperature. All other terms can be merged in parameter (a_i). The related values, along with other properties, are listed in Table 14.

[71] C. Carletti, F. Bjondahl, C. De Blasio, J. Ahlbeck, L. Järvinen, T. Westerlund. Modeling Limestone Reactivity and Sizing the Dissolution Tank in Wet Flue Gas Desulfurization Scrubbers. *Environ. Prog. Sustain. Energy* **2013**, *32*, 663-672.

Table 13 – Experimental conditions for the limestone dissolution kinetic experiments. Parameters used to perform the parametric study. $c_{S,0}$ = 6.66mol/m^3.

Test	Material	Size [μm]		T [K]	$c_{H+,0}$ [mol/m^3]	$S.R.$
1	Parainen	74-125	Small	293.15	3.43	1600
2	Parainen	74-125	Small	303.15	3.55	1600
3	Parainen	74-125	Small	313.15	3.72	1600
4	Parainen	74-125	Small	323.15	2.89	1600
5	Parainen	212-250	Large	293.15	3.53	1600
6	Parainen	212-250	Large	303.15	3.89	1600
7	Parainen	212-250	Large	313.15	3.83	1600
8	Parainen	212-250	Large	323.15	3.81	1600
9	Wolica	74-125	Small	293.15	3.27	1600
10	Wolica	74-125	Small	303.15	3.56	1600
11	Wolica	74-125	Small	313.15	3.91	1600
12	Wolica	74-125	Small	323.15	2.85	1600
13	Wolica	212-250	Large	293.15	3.41	1600
14	Wolica	212-250	Large	303.15	3.46	1600
15	Wolica	212-250	Large	313.15	3.96	1600
16	Wolica	212-250	Large	323.15	4.00	1600
17	Wolica	212-251	Large	323.15	3.84	1800
18	Wolica	212-252	Large	323.15	3.81	1200
19	Wolica	212-253	Large	323.15	3.83	800

Table 14 – Physical properties used to interpret the limestone dissolution kinetics in acidic environment.

	Value	*Unit*		*Value*	*Unit*
s	2	-	λ_{+}^{0} (H^+)	349.8	(A/m^2) (V/m) (g-equiv/m^3)
$c_{S,*}$	0.14	mol/m^3	z_+ (H^+)	1	-
MW_S	100.09	g/mol	λ_{-}^{0} (CO_3^{2-})	44.5	(A/m^2) (V/m) (g-equiv/m^3)
ρ_S	2930	kg/m^3	z_- (CO_3^{2-})	2	-
τ	1	s	a_{H+}	$3.12 \cdot 10^{-11}$	m^2/s/K
			a_S	$4.78 \cdot 10^{-12}$	m^2/s/K

Further details can be found in **Publication VI**.

All the experimental data collected at the same stirring rate, independent of the nature of the limestone, the particle size and temperature, were used for parameter estimation.

It is important to underline that the novelty of the current approach is to have one generic model covering a broad range of experimental conditions. In the literature in most cases the authors need either a complex kinetic expression or separate the dependencies to properly describe the data. We surmounted this problem with our model, making the obtained parameters more physically meaningful.

The results of the parameter estimation are reported in Table 15, highlighting that the parameters having reasonable confidence intervals and their mutual correlation is suppressed.

Table 15 – Estimated parameters for the limestone dissolution in acidic environment (tests 1-16 of Table 13).

Parameter	**Value**	**95% Confidence Interval**
Ea [J/mol]	$4.03 \cdot 10^4$	$0.23 \cdot 10^4$
k(293.15K) [$m^3/(mol \cdot s)$]	$2.48 \cdot 10^5$	$0.12 \cdot 10^5$
α [-]	50.36	0.75

Correlation Matrix			
	E_a	k	α
E_a	1.00		
k	0.54	1.00	
α	0.65	0.48	1.00

The obtained activation energy is higher than the ones reported for the Langmuir approach[71] (40kJ/mol for the present study vs 16-21kJ/mol for Wolica and 16.5-17.9kJ/mol for Parainen limestone). The result is encouraging, because low activation energy values are often an indication that the system is strongly influenced by mass transfer limitations. By considering that the new model describes more adequately the true physics of the system, including eventual mass transfer limitations, therefore the estimable values are expected to be more realistic. Therefore, a model characterized by reliable description of the involved physical phenomena leads to a more accurate kinetic investigation of the involved reaction.

The fits obtained for the experiments performed with the Parainen and Wolica limestone samples are reported in Figure 16.

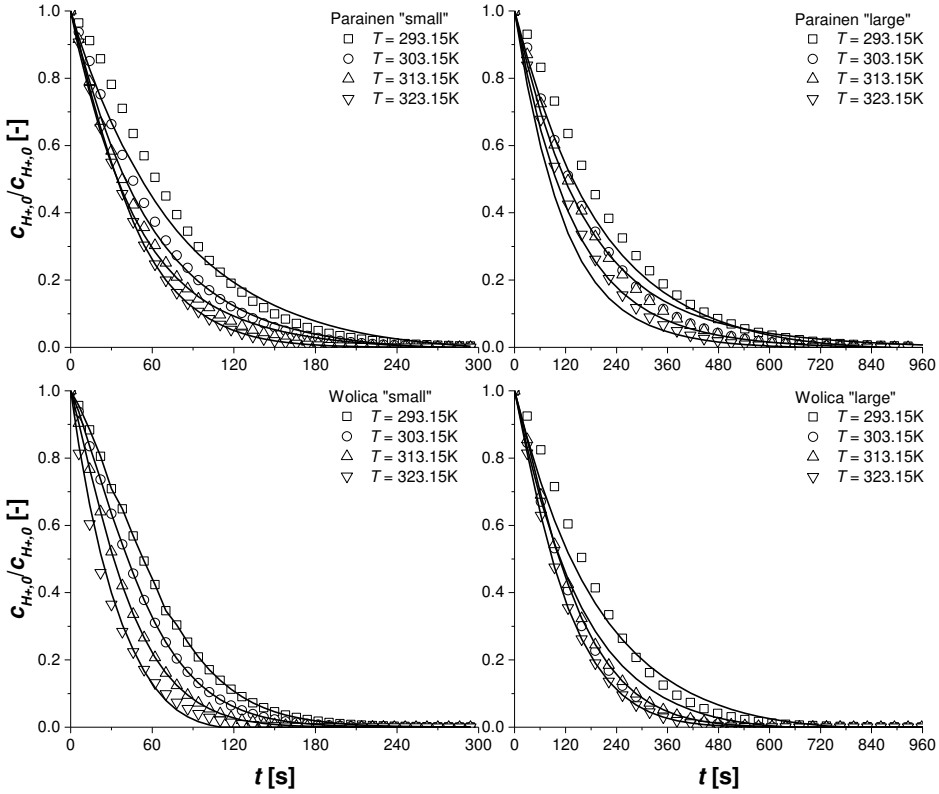

Figure 16 – Dimensionless proton concentration profiles for the limestone dissolution experiments performed at different temperatures, limestone type and dimensions. Stirring rate was fixed at 1600rpm.

As it can be seen, a good fit of the model to all the experimental data was obtained for the entire experimental domain.

Another new result was obtained in interpreting also the kinetic curves performed at different stirring rates and 50°C by using the "small" Wolica limestone sample (tests 16-19 of Table 13). The dimensionless mixing parameter (α) was estimated for each curve, by fixing the kinetic parameters. The trend of the estimated parameters vs the stirring rate is reported in Figure 17A.

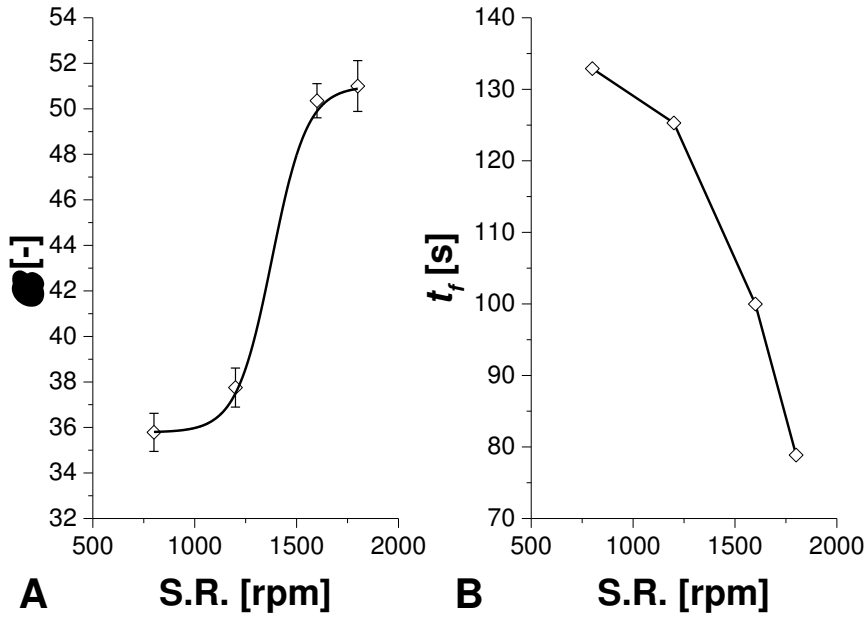

Figure 17 – A. Trend of the estimated dimensionless mixing parameter (α) as a function of the stirring rate. B. Time at the inflection point (t_f) for the contribution analysis.

By increasing the stirring rate, an increase of the stirring parameter (α) was observed until reaching approximately a plateau, which is in line with the observations of Carletti et al.[71]. From the contribution analysis of these experiments, it is possible to plot the time to the inflection point (t_f) against the stirring rate (Figure 17B). This point represents clearly the shift from the film to the bulk dominating regime.

The time of the inflection point decreases by increasing the stirring rate. At low stirring rates, the overall kinetics is dominated by the mass transfer limitation in the liquid film for a long period during an experiment, while at higher stirring rates, the overall kinetics is dominated by the chemical reaction itself. This aspect is of high importance in the design and scale-up reactors for solid-liquid processes. Stirring in large vessels requires a high energy input. Dedicated simulations could indicate a minimum stirring rate which would be required for the operation under kinetic control, leading to well-designed and less expensive reactors.

5.5 Conclusions

The developed Extended Shrinking Film Model (E.S.F.M.) is certainly an advancement in the field of fluid-solid reaction modeling when the solid is a dissolving reactant. The mass balance equations describing the model were derived to simulate the film thickness varying with the reaction time.

A preliminary parametric investigation for a bimolecular reaction was conducted showing the high potential of the model and covering a wide range of physical cases. Relevant concentration profiles were obtained in all the cases.

Limestone dissolution in acidic environment was used as a case study to verify the model. Experimental data published in the literature were correctly interpreted by performing parameter estimation on an extensive set of experiments covering different operation parameters, including the stirring rate. The intrinsic reaction kinetics was revealed, giving reliable parameters with a molecular reaction rate expression, concluding that the low apparent activation energies often reported in literature are mainly due to film diffusion limitations and not by intrinsic chemical kinetics.

From the obtained results, it can be concluded that the model has general features, applicable to a wide range of reactive systems in which a solid reactant is dissolved with time. The model has a high flexibility. For example, it could be applied to enamel dissolution in acidic environment, a system particularly important for dental care[72], or quartz dissolution in NaCl solutions for geological investigation of the evolution of diverse earth processes[73]. The model could be the basis to develop a crystallization kinetic model. Evidently, further efforts should be paid on this topic.

---

[72] J.A. Gray. Kinetics of Enamel Dissolution During Formation of Incipient Caries-Like Lesions. *Arch. Oral Biol.* **1966**, *11*, 397-421.

[73] P.M. Dove. The Dissolution Kinetics of Quartz in Sodium Chloride Solutions At 25° To 300°. *American Journal of Science* **1994**, *294*, 665-712.

List of symbols

a_p	Surface area-to-volume ratio, [m^2/m^3]
a', b'	Coefficients in the correlation for Sherwood number, [-]
a_i	Diffusivity coefficient, [$m^2/(s \cdot K)$]
ADn	Dimensionless parameter (n=1 to 4), [-]
c	Concentration, [mol/m^3]
D	Diffusion coefficient, [m^2/s]
D^0_{AB}	Ion diffusivity, [m^2/s]
d	Particle diameter (=2R), [m]
Ea	Activation energy, [J/mol]
F	Faraday, 96.5 [C/g-equiv]
k	Reaction rate constant, [$m^3/(mol \cdot s)$]
k_L	Mass transfer coefficient, [m/s]
M	Molar mass, [kg/mol]
M_p	Particle mass, [kg]
MW	Molecular weight, [g/mol]
N	Diffusion flux, [$mol/(m^2 \cdot s)$]
n_j	Amount of substance, [mol]
n_p	Particles number, [-]
R	Particle radius, [m]
R_0	Particle radius at t=0, [m]
r	Radial coordinate, [m]
r_j, r_j'	Generation rate, [$mol/(m^3 \cdot s)$]
$S.R.$	Stirring rate, [rpm]
s	Shape factor, [-]
T	Temperature, [K]
t	Time, [s]
V	Volume, [m^3]
x	Dimensionless film coordinate, [-]
X_R	Particle radius conversion, [-]
y	Dimensionless concentration, [-]
y'	Dimensionless concentration in the bulk phase, [-]
z_+,z_-	Ion valence, [-]

Greek symbols

α	Dimensionless number, [-]
α', β'	Exponent in the correlation for Sherwood number parameter in rate equation, [-]
δ	Film thickness, [m]
ε	Dissipated energy, [W/kg]
θ	Dimensionless time, [-]
κ	Contribution, [mol/s]
λ	Normalized contribution, [-]
λ^0_+, λ^0_-	Limiting zero concentration ionic conductance, [(A/m^2) (V/m) (g-equiv/m^3)]
υ	Kinematic viscosity, [m^2/s]
ρ	Density, [kg/m^3]
τ	Characteristic reaction time, [s]

Dimensionless numbers

Re	Reynolds number, [-]
Sc	Schmidt number, [-]
Sh	Sherwood number, [-]

Subscripts and superscripts

B	Bulk phase
f	Inflection point
F	Film
i	Liquid-phase and general component index
j	Solid-phase component index
k	Reaction rate index
L	Liquid phase
P	Particle
0	Initial quantity
*	Saturated state

Chapter 6 – Conclusions

"Mathematics is the cheapest science. Unlike physics or chemistry, it does not require any expensive equipment. All one needs for mathematics is a pencil and paper."

George Pólya, Mathematical People, 1985

Conclusions

Different modelling approaches were presented in the current thesis. Some general conclusions can be drawn from the obtained results.

The developed general three-phase continuous model showed good performances and a high potential. Despite the complexity of the system, the model led to reasonable computation times also in cases when parameter estimation was performed. Concentration profiles along each calculation coordinate were obtained, and eventual catalyst deactivation effects were included. The model can be considered as a generic one being applicable for the development of different kinds of sub-models for multiphase chemical reaction engineering.

For this purpose, different sub-models were developed. Two microreactor models were used to interpret experimental data on the ethylene oxide synthesis in microreactors. Due to the reliable interpretation of physical phenomena, it was possible to describe all available experiments, conducted at a wide range of conditions. The two models demonstrated that microreactors cannot in real cases be described by a simple approach, such as a plug-flow fluid dynamics model.

A fluid-solid packed bed reactor was developed for the partial oxidation of ethanol. The experimental data collected by our group were well described and a sensitivity study was conducted to show the influence of the main conditions and process parameters.

Finally, a shrinking particle model for fluid-solid reactions was developed to describe limestone dissolution experiments carried out in an acidic environment. By developing this model, we solved the problem related to moving boundary conditions, represented by the film thickness surrounding the solid particle, which shrinks as the reaction proceeds. With this model, it was possible to describe adequately all the experimental data collected at a wide range of operation conditions. The intrinsic kinetics of the dissolution process was revealed and reliable kinetic and mass transfer parameters were obtained.

A general conclusion is that by using advanced models in chemical reaction engineering, a significant part of the fluid-solid systems problems can be covered, therefore the present work can be of high utility value for researchers in both academia and industry in the design of future laboratory-scale and industrial-scale reactors.

The simulation of fluid-solid reactors is the topic of this thesis. Starting from a general non-isothermal three-phase tubular reactor model, several sub-models were derived and tested:

Trickle-bed reactor:	arabinose hydrogenation
Microreactor:	ethylene oxide synthesis
Packed-bed reactor:	ethanol oxidation

A special liquid-solid system was modelled, where the solid acts as reactant, diminishing in size as the reaction progresses.

ISBN 978-952-12-3598-6